The American Journal of Pathology, Vol. 193, No. 1, January 2023

ELSEVIER

The American Journal of PATHOLOGY

ajp.amjpathol.org

TUMORIGENESIS AND NEOPLASTIC PROGRESSION

Esr1 but Not *CYP19A1* Overexpression in Mammary Epithelial Cells during Reproductive Senescence Induces Pregnancy-Like Proliferative Mammary Disease Responsive to Anti-Hormonals

Priscilla A. Furth,*† Weisheng Wang,* Keunsoo Kang,‡ Brendan L. Rooney,* Grace Keegan,* Vinona Muralidaran,* Xiaojun Zou,* and Jodi A. Flaws§

From the Departments of Oncology and Medicine,† Georgetown University, Washington, District of Columbia; the Department of Microbiology,‡ College of Science and Technology, Dankook University, Cheonan, Republic of Korea; and the Department of Comparative Biosciences,§ University of Illinois Urbana-Champaign, Urbana, Illinois*

Accepted for publication September 16, 2022.

Address correspondence to Priscilla A. Furth, M.D., Georgetown University, 3970 Reservoir Rd. N.W., Research Bldg., Room E407A, Washington, DC 20057.
E-mail: paf3@georgetown.edu.

Molecular-level analyses of breast carcinogenesis benefit from *vivo* disease models. Estrogen receptor 1 (*Esr1*) and cytochrome P450 family 19 subfamily A member 1 (*CYP19A1*) overexpression targeted to mammary epithelial cells in genetically engineered mouse models induces largely similar rates of proliferative mammary disease in prereproductive senescent mice. Herein, with natural reproductive senescence, *Esr1* overexpression compared with *CYP19A1* overexpression resulted in significantly higher rates of preneoplasia and cancer. Before reproductive senescence, *Esr1*, but not *CYP19A1*, overexpressing mice are tamoxifen resistant. However, during reproductive senescence, *Esr1* mice exhibited responsiveness. Both *Esr1* and *CYP19A1* are responsive to letrozole before and after reproductive senescence. Gene Set Enrichment Analyses of RNA-sequencing data sets showed that higher disease rates in *Esr1* mice were accompanied by significantly higher expression of cell proliferation genes, including members of prognostic platforms for women with early-stage hormone receptor—positive disease. Tamoxifen and letrozole exposure induced down-regulation of these genes and resolved differences between the two models. Both *Esr1* and *CYP19A1* overexpression induced abnormal developmental patterns of pregnancy-like gene expression. This resolved with progression through reproductive senescence in *CYP19A1* mice, but was more persistent in *Esr1* mice, resolving only with tamoxifen and letrozole exposure. In summary, genetically engineered mouse models of *Esr1* and *CYP19A1* overexpression revealed a diversion of disease processes resulting from the two distinct molecular pathophysiological mammary gland—targeted intrusions into estrogen signaling during reproductive senescence. *(Am J Pathol 2023, 193: 84—102; https://doi.org/10.1016/j.ajpath.2022.09.007)*

Breast cancer continues to be a world-wide challenge.[1] In 2020, it was the most diagnosed malignancy in women. In spite of all the current treatment options, it continues to lead to significant morbidity and mortality. Disparities between populations for access to optimal medical care remain a persistent problem across the globe. Understanding the pathophysiology of breast cancer and dissection of disease pathways could lead to more effective prevention, screening, and early detection strategies.

Unrestrained cell proliferation is an established risk factor for cancer generation, including breast cancer.[2] Estrogen signaling pathways play a direct role in breast epithelial cell

Supported by NIH UH3CA213388 (P.A.F.) and NIH P30CA051008 (P.A.F.).

Disclosures: None declared.

Current address of W.W., Department of Microbiology, Immunology and Tropical Medicine, George Washington University, Washington, DC.

https://doi.org/10.1016/j.ajpath.2022.09.007

growth-inducing carcinogenesis as well as influencing the surrounding stromal and immunologic environment.[3,4] The increased levels of estrogen receptor α (ER) and aromatase expression found in post-menopausal breast tissue are posited to contribute to the increased risk of breast cancer in post-menopausal women.[5,6] ER contributes to cell proliferation of mammary epithelial cells via both genomic and non-genomic actions.[7] ER genomic action activates signaling pathways linked to regulation of cell proliferation, including myc proto-oncogene basic helix-loop-helix transcription factor (MYC), cyclin D1, the cyclin E (CCNE1)−cyclin-dependent kinase 2−cyclin-dependent kinase inhibitor 1a complex, and cell survival, including bcl2 apoptosis regulator and bcl2-like 1.[8,9] Proteins implicated in nongenomic extra-nuclear pathway ER-mediated cell proliferation pathways include insulin-like growth factor I receptor, matrix metallopeptidase 2, matrix metallopeptidase 9, epidermal growth factor receptor (EGFR), mitogen-activated protein kinase, src homology 2 domain-containing adaptor protein 1, growth factor receptor-bound protein 2, and son of sevenless Ras/Rac guanine nucleotide exchange factor 1.[10,11] Aromatase, encoded by the cytochrome P450 family 19 subfamily A member 1 (*CYP19A1*) gene in humans, acts as the rate-limiting enzyme for conversion of testosterone to estrogen.[12] Breast-localized aromatase expression has been linked to increased breast cancer risk through ER-dependent genomic and nongenomic mechanisms as well as ER-independent actions that include direct DNA damage.[11,12]

Anti-hormonal agents with positive results for primary breast cancer prevention in high-risk women include both selective ER modulators, such as tamoxifen and raloxifene, as well as aromatase inhibitors.[13−15] Selective ER modulator−associated adverse effects are one reason research continues into assessment of aromatase inhibitors as well as other agents and preventive interventions.[16,17] Pathways that may modify response to anti-hormonal agents, such as interferon-related pathways, are also a research focus.[18−21]

Studies in breast cancer pathogenesis may determine a molecular prognostic risk classification system for primary cancer occurrence, or secondary cancer recurrence, of different types of breast cancers.[22,23] In particular, the Prediction Analysis of Microarray 50 (PAM50) risk of recurrence score has been useful for evaluating prognosis of early-stage hormone receptor−positive/human epidermal growth factor receptor 2-negative breast cancer in women, including in post-menopausal women.[24,25] Development of such a risk classifier may need to incorporate multiple parameters, including transcriptome information.[26−28] For example, the PAM50 panel includes genes linked to genomic (*MYC* and *CCNE1*) and nongenomic (*EGFR*) ER-mediated mechanisms of cell proliferation from cell culture studies. Parallels in transcription between human and mouse models have been used to study disease pathogenesis in the natural setting.[29,30]

Breast cancer−related mouse models enable investigation of disease pathophysiology within the context of physiological endocrine and immunologic function.[31−33] In a mouse model of reproductive aging, both mouse mammary tumor virus−reverse tetracycline−controlled transactivator/tet-operator (tet-op)−estrogen receptor 1 (*Esr1*) and mouse mammary tumor virus−reverse tetracycline−controlled transactivator/*CYP19A1* (*CYP19A1*) mice show elevated expression levels of *Esr1* and *Pgr*.[19,34] Preneoplastic lesions in both models are typically estrogen receptor α positive (ER^+) in prereproductive senescent mice, but invasive cancers are either negative (ER^-) or have a low percentage of ER positivity in the cancers.[34−36] Prereproductive senescent *Esr1*, but not *CYP19A1*, mice are relatively resistant to tamoxifen,[35] which is linked to increased activation of an interferon regulatory factor 7 (IRF7)-STAT1 pathway in mammary epithelial cells.[19]

When performing transcriptional studies in whole mammary tissue, expression levels of luminal [keratin (*Krt*) *7*, *Krt8*, *Krt18*, and *Krt19*) and basal (*Krt5* and *Krt14*) cytokeratins can be used for assessment of relative mammary epithelial cell content in samples.[37−39] Levels have to be understood in context, as keratins such as *Krt5* and *Krt14* can both contribute to regulation of cell proliferation and exhibit higher expression levels in proliferative cells.[37,40] Expression levels of *Krt5*, *Krt14*, and *Krt17* are included in the PAM50 risk panel.[25]

In mice, the major source of estrogen production is the granulosa cells of the ovarian follicles.[41] Reproductive senescence is initiated by loss of ovarian follicles with coincident decrease in systemic estrogen levels. Ovarian follicle development, including numbers and types of follicles, is assessed histologically in ovarian tissue samples as a measure of ovarian follicle reserve and reproductive function.[42,43] When ovarian follicle numbers are low, systemic estrogen levels are also low.[44]

The current study was initiated to determine whether altering the induction of *Esr1* and *CYP19A1* transgene expression to after reproductive maturity, and then postponing anti-hormonal therapy until reproductive senescence, could differentially impact disease pathophysiology and anti-hormonal responsiveness in the two models. Aging is the greatest risk factor for developing breast cancer.[45−47] Studies indicate that >80% of cases occur in women aged >50 years, 50% in women aged >65 years, and 21% in women aged >70 years.[48−51] Several mechanisms have been suggested to account for this relationship, including alterations in progenitor cell populations, age-associated somatic mutation, changes in the microenvironment, and epigenetic alterations.[51] Yet, despite the association of aging with breast cancer, most mouse model studies of breast cancer genetics are conducted before reproductive senescence.[32,52−54] Notable exceptions include mice with cyclin D1, nuclear receptor coactivator 3 (alias amplified in breast cancer 1 protein; AIB1), or prolactin overexpression or *Stat1* deletion, where most invasive cancers arise with or after reproductive senescence.[55−58] A unique aspect of this study is the use of conditional transgene models. Genetic alterations in most nonconditional models are present from birth and active during early during reproductive life. In this study, the *Esr1* and *CYP19A1* transgenes were induced at

middle age and continued through reproductive senescence as the mice aged. The impact of two different anti-hormonals, tamoxifen and letrozole, both prescribed for breast cancer risk reduction in post-menopausal women, was studied in the mice during reproductive senescence. Significantly, the study revealed a differential impact of *Esr1* overexpression versus *CYP19A1* overexpression at this age. Compared with *CYP19A1* mice, *Esr1* mice exhibited a significantly higher proliferative transcriptional response, reminiscent of pregnancy, with parallels to the human PAM50 risk profile that associated with increased prevalence of preneoplasia and cancer. *Esr1*-induced proliferative changes resolved to levels approximating those found in the less-proliferative *CYP19A1* mice following tamoxifen or letrozole. The study demonstrated that increased breast cancer risk due to ER or aromatase overexpression can be effectively modeled, and interventions can be tested in aging mice.

Materials and Methods

Mouse Models

The Georgetown University (Washington, DC) Institutional Animal Care and Use Committee approved the animal research protocol, and all regulations concerning the use of animals in research were carefully adhered to throughout the conduct of the experiments. Mouse mammary tumor virus–reverse tetracycline–controlled transactivator/tet-op–*Esr1* and mouse mammary tumor virus–reverse tetracycline–controlled transactivator/tet-op-*CYP19A1* mice on a C57Bl/6 background were bred in the Georgetown University Department of Comparative Medicine facility, genotyped at weaning (Transnetyx, Inc., Cordova, TN), and sequentially placed through the four different experimental cohorts for each genotype until each cohort was filled with end point cohort size planned for $n = 20$. Twelve C57Bl/6 wild-type mice were included as a reference cohort for ovarian follicle counts between 2 and 5 months of age ($n = 2$ age 2 months, $n = 3$ age 3 months, $n = 5$ age 4 months, and $n = 2$ age 5 months). A total of 10% and 25% losses from the cohorts were predicted for the 18- and 20-month end point cohorts, respectively (*https://www.nia.nih.gov/research/dab/aged-rodent-colonies-handbook/animal-information*, last accessed September 17, 2022). All cohorts were raised on Department of Comparative Medicine standard laboratory mouse chow until 12 months of age, when they were switched to diet containing 200 mg doxycycline per kilogram food (Bio-Serv, Flemington, NJ) for transgene induction. One cohort from each genotype was euthanized for the age 18-month end point. The three 20-month end point cohorts from each genotype were subjected to anesthesia and surgical s.c. pocket formation with placement of no pellet, a tamoxifen pellet (25 mg/60-day release), or a letrozole pellet (2.5 mg/60-day release; Innovative Research of America, Sarasota, FL) at age 18 months and followed up until age 20 months, when they were euthanized. Euthanasia was conducted according to the approved animal protocol using CO_2 inhalation followed by cervical dislocation. All mice were individually followed up for development of disease or cage death as they were aged to the 18 and 20 months of age end points. Mice were euthanized before the age 18- or 20-month experimental end points according to the approved research protocol for pain/distress/infection unresponsive to treatment, severe lethargy or weakness, severe neurologic signs, severe respiratory distress, total tumor burden >2 cm, weight loss ≥15% of body weight, or wounds refractory to treatment. Cage deaths were unpredicted spontaneous deaths lacking an identifiable cause. Numbers of mice in each cohort were as follows: *Esr1*: 18 month $n = 26$ entered, $n = 3$ early necropsy, $n = 3$ cage death, end point $n = 20$ (77% survival); 20 month $n = 33$ entered, $n = 9$ early necropsy, $n = 5$ cage death, end point $n = 19$ (58% survival); 20 month with tamoxifen $n = 32$ entered, $n = 4$ early necropsy, $n = 4$ cage death, end point $n = 24$ (75% survival); 20 month with letrozole $n = 32$ entered, $n = 11$ early necropsy, $n = 1$ cage death, $n = 20$ (62% survival). *CYP19A1*: 18 month $n = 22$ entered, end point $n = 22$ (100% survival); 20 month $n = 32$ entered, $n = 5$ early necropsy, $n = 9$ cage death, end point $n = 18$ (56% survival); 20 month with tamoxifen $n = 31$ entered, $n = 5$ early necropsy, $n = 3$ cage death, end point $n = 23$ (74% survival); 20 month with letrozole $n = 33$ entered, $n = 2$ early necropsy, $n = 7$ cage death, $n = 24$ (73% survival). Mean weights ± SEM at end point for each cohort were as follows: *Esr1*: 18 month 41 ± 3 g, 20 month 50 ± 3 g, 20 month with tamoxifen 45 ± 3 g, 20 month with letrozole 46 ± 4 g. *CYP19A1*: 18 month 32 ± 1 g, 20 month 31 ± 1 g, 20 month with tamoxifen 31 ± 1 g, 20 month with letrozole 33 ± 1 g.

To validate transgene expression in the different cohorts, thoracic (number 2) mammary glands were flash frozen in liquid nitrogen and stored at −80°C until processing. Randomly selected glands from each cohort were thawed in Invitrogen Trizol reagent (ThermoFisher Scientific, Waltham, MA) and homogenized using a Qiagen Tissuruptor and Qiashredder (Qiagen, Hilden, Germany). RNA was then isolated using Direct Zol RNA miniprep kit (Zymo Research, Irvine, CA), quantified on a Qubit 2.0 Fluorometer (Qiagen) and analyzed for RNA integrity using the Agilent 2100 Bioanalyzer (Agilent, Santa Clara, CA). RNA (1 μg) was used to generate cDNA with the High Capacity RNA to cDNA kit (Applied Biosystems, Waltham, MA), and RT-PCR was conducted using Platinum Taq DNA Polymerase (Invitrogen, Waltham, MA). For *tet-op–Esr1*, two unique primer pairs were used and expression was normalized to β-actin expression levels[59]: Sp3 pair: 5′-CCACACCAGCCACCACCTTC-3′ (forward) and 5′-CCACTTCAGCACATTCCTTA-3′ (reverse); and Sp4 pair: 5′-GATGAGACAGCACAACAACC-3′

(forward) and 5′-CAAAGGCATGGAGCATCTCT-3′ (reverse); predicted sizes were 287 and 385 bp, respectively. For *tet-op−CYP19A1*, one unique primer set was used and expression was normalized to β-actin expression levels[34]: tet-op−CYP19A1: 5′-CCTTGCACCCA-GATGAGACT-3′ (forward) and 5′-GACAGCACAA-CAACCAGCAC-3′ (reverse); predicted size was 134 bp. Endogenous mouse β-actin was 5′-ATCGTGGGCCGCCCTAGGCA-3′ (forward) and 5′-TGGCCTTAGGGTTCAGAGGG-3′ (reverse); predicted size was 244 bp. PCR amplicons were run on 2% agarose E-gels (Invitrogen) and imaged using blue fluorescence on the Amersham Imager 600 (GE HealthCare, Chicago, IL). Adobe Photoshop (San Jose, CA) was used to calculate relative pixel intensities for the bands from each image, with normalization of transgene expression levels to β-actin expression level individually for each sample. Percentage relative transgene expression was calculated across all four cohorts for each genotype, setting the age 18-month expression levels at 100%.

Mammary Gland Whole Mount Evaluation

Carmine-alum−stained mammary gland whole mounts were prepared from one inguinal (number 4) mammary gland from each necropsied mouse at end point using standard procedures.[60] Whole mounts were visually examined, and images were taken at ×0.5 utilizing a Nikon Eclipse E800M microscope with Nikon DMX1200 software (Nikon Instruments, Inc., Melville, NY). Four independent observers (P.A.F., W.W., B.L.R., and V.M.) blindly scored whole mounts for branching structures (secondary versus tertiary),[61] lobular growth (presence versus absence),[62] and hyperplastic alveolar nodules (HANs; number present).[63] The final score was the majority score. In the case of a tie, images were re-examined by P.A.F. and a final score was set. Glands were defined as hyperplastic when at least one HAN was present in the whole mount. Presence or absence of dense uniform pregnancy-like growth patterns was scored by P.A.F. Mammary gland images were digitally scored for mean relative density utilizing an automated program that uses mean pixel intensity to represent mammary density.[64] Lower-density scores correspond to lower mean pixel intensity scores and higher mammary gland density. Higher-density scores correspond to higher mean pixel intensity and lower mammary gland density.

Histology and ER α Immunohistochemistry

Inguinal (number 4) mammary glands were fixed in 10% neutral formalin solution and embedded in paraffin, and tissue sections (5 μm thick) were utilized for hematoxylin and eosin (H&E) staining and ER α immunohistochemistry. Relative cellularity was assessed on H&E-stained mammary mid-gland longitudinal sections. Low cellularity was defined as ≤10 cell clusters, moderate cellularity was defined as 11 to 20 clusters, and high cellularity was defined as >20 clusters. A cell cluster was defined as five or more cells. ER α protein was detected utilizing rabbit polyclonal anti−estrogen receptor α (catalog number 06-935; Millipore Sigma, Burlington, MA), 1:4800, 1 hour, room temperature. Before application of primary antibody, heat-induced epitope retrieval was performed by immersing tissue sections at 98°C for 20 minutes in 10 mmol/L citrate buffer (pH 6.0) with 0.05% Tween, followed by treatment with 3% hydrogen peroxide and 10% normal goat serum (10 minutes each). Following primary antibody exposure, slides were exposed to a horseradish peroxidase−labeled polymer [30 minutes; EnVision+ System-HRP Labeled Polymer Anti-Rabbit; K4003 (Agilent, Dako, Carpinteria, CA)] and 3′-diaminobenzidine (5 minutes; Agilent, Dako) and counterstained with hematoxylin (Harris Modified Hematoxylin; Fisher Scientific, Hampton, NH). H&E slides were read blindly by two independent readers (P.A.F. and W.W.). ER α immunohistochemistry was read by P.A.F. Digital images were taken at ×40 utilizing a Nikon DMX1200 camera mounted on a Nikon Eclipse E800M microscope.

RNA-Sequencing Analysis and Visualizations

Thoracic (number 2) mammary glands were flash frozen in liquid nitrogen and stored at −80°C until processing. Glands were thawed in Invitrogen Trizol reagent (ThermoFisher Scientific) and homogenized using a Qiagen Tissuruptor and Qiashredder. RNA was then isolated using Direct Zol RNA miniprep kit (Zymo Research), quantified on a Qubit 2.0 or 4.0 Fluorometer (Qiagen) and analyzed for RNA integrity using the Agilent 2100 Bioanalyzer. Indexed, single-index sequencing libraries were prepared from 1 μg ribosome depleted total RNA using TruSeq Stranded Total RNA Library Preparation Human/Mouse/Rat (Illumina, San Diego, CA). Sequencing was performed using the Illumina NextSeq 550, SE 75-bp read length; minimum reads ≥50 million per sample. Sequencing quality was checked using FastQC processing version 0.11.9 (*https://www.bioinformatics.babraham.ac.uk/projects/fastqc*, last accessed August 7, 2022). Contaminated adaptor and/or low-quality portions of sequenced reads were trimmed using Trim Galore version 0.6.5 (*https://github.com/FelixKrueger/TrimGalore*, last accessed August 7, 2022). Trimmed reads were aligned to the reference mouse genome (mm10), using STAR version 2.7.9a.[65] Batch effect was normalized using RUVSeq version 1.26.0 with the RUVg method.[66] Normalized expression levels were estimated by means of transcripts per million using RSEM version 1.3.1.[67] Differentially expressed genes (DEGs) between genotypes at each end point were identified using DESeq2.[68] Genes were considered statistically significantly differentially expressed when the adjusted *P* value was <0.05. Protein-coding DEGs between models at each end point were identified, and numbers were visualized

as expressed higher in *Esr1* versus *CYP19A1* mice using bar graphs with each group analyzed independently for enrichment in HALLMARK gene sets (Gene Set Enrichment Analysis, Molecular Signatures Database version 7.5.1, updated January 2022, last accessed July 31, 2022).[69,70] The top three gene sets by false discovery rate q-value were visualized using bar graphs. Because the highest numbers of DEGs between the two models occurred at the 20-month end point with identification of cell proliferation–related enriched HALLMARK gene sets in the *Esr1* mice, DEGs from this group were selected to identify overlaps with the Prosigna PAM50 gene set.[22] Transcripts per million for overlapping genes were presented by bar graph, categorized by cell proliferation versus estrogen response–related genes. A heat map illustrating changes in relative gene expression for these genes across all four end points for both models was constructed (GraphPad Prism version 9.3.1; GraphPad Software, San Diego, CA). A total of nine DEGs at the 20-month end point identified as members of both the PAM50 profile are known to exhibit pregnancy stage–related changes in gene expression.[11] Heat maps of these nine as well as 34 additional genes regulated during normal pregnancy-related development from National Center for Biotechnology Information's Gene Expression Omnibus GSE70440 (*https://www.ncbi.nlm.nih.gov/geo/query/acc.cgi?acc=GSE70440*, last accessed September 17, 2022)[71] were constructed to visualize relative expression levels during normal pregnancy[28] in comparison to relative expression levels across time and treatment condition for the eight experimental cohorts (GraphPad Prism version 9.3.1). A heat map of 12 *Irf7-Stat1* immune-related genes linked to tamoxifen resistance,[19] five HALLMARK_INFG_RESPONSE, and four HALLMARK_TNFA_SIGNALING_VIA_NFKB DEGs identified at age 12 months in *Esr1* and *CYP19A1* mice with transgene induction at age 12 months was constructed to illustrate the differences in relative levels of gene expression between the tamoxifen-resistant 12-month–old *Esr1* mice and tamoxifen-responsive 18- and 20-month–old *Esr1* and 12-, 18-, and 20-month–old *CYP19A1* mice (GraphPad Prism version 9.3.1). The new data discussed in this publication were deposited in National Center for Biotechnology Information's Gene Expression Omnibus[72] and are accessible through series accession number GSE201326 (*https://www.ncbi.nlm.nih.gov/geo/query/acc.cgi?acc=gse201326*, last accessed August 7, 2022).

Ovarian Follicle Counts

Ovaries were subjected to histologic evaluation of healthy and unhealthy follicles.[42,43] The ovaries were fixed in paraformaldehyde, embedded in paraffin, and sectioned every 8 μm using a microtome. After sectioning, slides were stained with H&E. Every 10th section of the ovary was used to count the total number of primordial follicles, primary follicles, preantral follicles, antral follicles, atretic follicles, and abnormal follicles. All sections were examined without knowledge of treatment group. Primordial follicles were defined as follicles with an oocyte, surrounded by a single layer of squamous granulosa cells. Primary follicles were defined as follicles that consist of an oocyte, surrounded by a single layer of cuboidal granulosa cells. Preantral follicles were defined as follicles containing an oocyte, surrounded by multiple layers of cuboidal granulosa cells and theca cells. Antral follicles were defined as follicles that consist of an oocyte, surrounded by numerous layers of cuboidal granulosa cells, theca cells, and a fluid-filled antrum. Atretic follicles were counted as preantral or antral follicles that contain $\geq$10% number of apoptotic bodies. Abnormal follicles included follicles with double oocytes and/or fragmented nuclei. Preantral and antral follicles were required to have nuclear material present to avoid double counting. Total number of follicles and number and percentage of each type of follicle were recorded.

Statistical Analysis

Calculations of means and SEMs were performed utilizing GraphPad Prism version 9.3.1. Multiple unpaired *t*-tests were used to compare primordial, primary, preantral, antral, and atretic follicle counts; the Fisher exact test was used to determine if there were nonrandom associations between tertiary and secondary branching, presence and absence of lobular growth, HANs, or preneoplasia/cancer; and *U*-test was used to compare relative mean mammary gland density scores ($P < 0.05$ considered statistically significant; GraphPad Prism version 9.3.1). The Fisher exact, Freeman-Halton extension was used to determine if there were nonrandom associations between proportions of mice with cancer, preneoplasia, and normal findings between cohorts ($P < 0.05$ considered statistically significant; *http://vassarstats.net/fisher2x3.html*, last accessed August 7, 2022). Scatterplots and bar graphs were prepared utilizing GraphPad Prism version 9.3.1. Significance levels for specific comparisons are indicated by asterisks: $*P < 0.05$, $**P < 0.01$, $***P < 0.001$, and $****P < 0.0001$.

Results

Changes in Mammary Gland Morphology Induced by Reproductive Senescence in Mouse Models of Breast Cancer Risk Are Accentuated by Tamoxifen and Letrozole Exposure

The study design was intended to model how increased levels of *Esr1* and *CYP19A1* expression during menopause in women impact response to anti-hormonals, such as tamoxifen and letrozole, prescribed for breast cancer risk reduction. *Esr1* and *CYP19A1* transgenes targeted to mammary epithelial cells were induced at age 12 months, a time point corresponding to middle age in humans (*https://www.jax.org/research-and-faculty/research-labs/the-harrison-lab/gerontology/life-span-as-a-biomarker*, last accessed August 7, 2022).[73] At weaning, mice were divided into

four cohorts: one with an age 18-month end point and three cohorts with surgery at age 18 months for placement for tamoxifen or letrozole or no pellet placement and then followed for 2 months with end point at age 20 months (Figure 1A). Ovarian follicle counts were performed on mice from each cohort to assess ovarian reserves as a marker of reproductive senescence. All eight experimental cohorts demonstrated significantly fewer counts of all follicle types which were abnormal compared with young reproductive age wild-type mice (age 2 to 5 months), indicating that both the 18- and 20-month–old mice had entered into reproductive senescence (Figure 1B). Mammary gland whole mounts were used to assess branching, lobular growth morphology, and overall mammary gland density. Changes in branching structure were the least sensitive to reproductive senescence, with only *Esr1* mice exhibiting a significant decrease in the proportion of mice with tertiary branching between 18 and 20 months of age (Figure 2A). Significant reductions in lobular growth, accentuated in mice treated with either anti-hormonal, were found with progression through reproductive senescence (Figure 2B). A significant difference between the

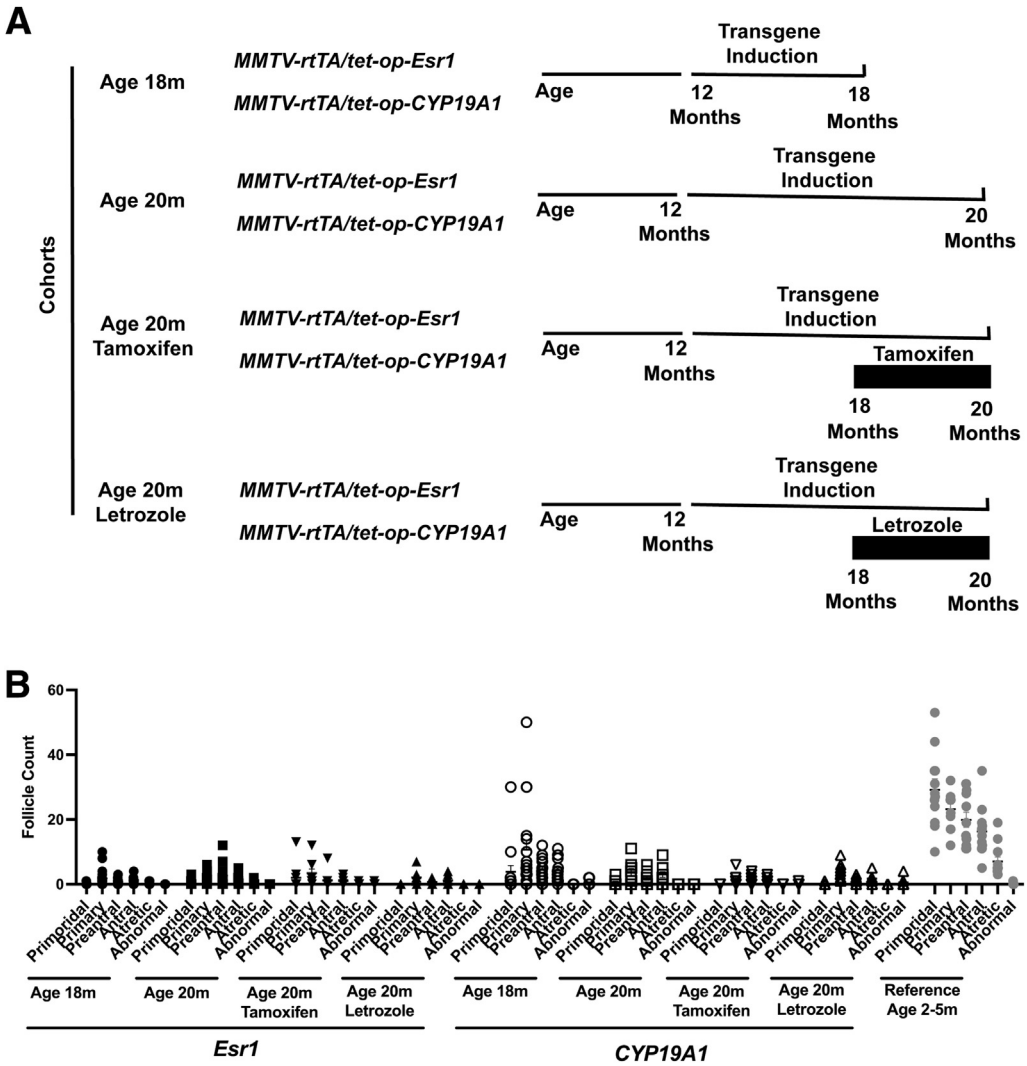

Figure 1 Experimental design and characterization of ovarian follicle counts during reproductive senescence at 18 and 20 months (m) of age. **A:** Study cohort design: *Esr1* and *CYP19A1* transgene expression was induced at age 12 months. The end point at age 18 months had no intervention. The end point at age 20 months was with s.c. pellet placement surgery at age 18 months for anti-hormonal exposure [none, tamoxifen (25 mg/60-day release), or letrozole (2.5 mg/60-day release)]. **B:** Scatterplots illustrate distribution of ovarian follicle counts of *Esr1* and *CYP19A1* mice at 18 and 20 months of age without and with tamoxifen or letrozole exposure. Follicle counts of wild-type mice at 2 to 5 months of age shown for reference. Black fill: *Esr1*. White fill: *CYP19A1*. **Circles:** age 18m ($n = 18$ *Esr1*, $n = 22$ *CYP19A1*). **Squares:** age 20m ($n = 11$ *Esr1*, $N = 10$ *CYP19A1*). **Inverted triangle:** age 20m with 2 months tamoxifen exposure ($n = 9$ *Esr1*, $n = 10$ *CYP19A1*). **Triangle:** age 20m with 2 months letrozole exposure ($n = 9$ *Esr1*, $n = 11$ *CYP19A1*). **Gray circles:** wild type ($n = 12$). Primordial, primary, preantral, antral, and atretic follicle counts significantly lower in all cohorts of 18- and 20-month–old mice compared with 2- to 5-month–old mice ($P < 0.005$, multiple unpaired *t*-tests, GraphPad Prism version 9.3.1). Data are presented as means ± SEM (**B**). MMTV, mouse mammary tumor virus; rtTA, reverse tetracycline–controlled transactivator; tet-op, tet-operator.

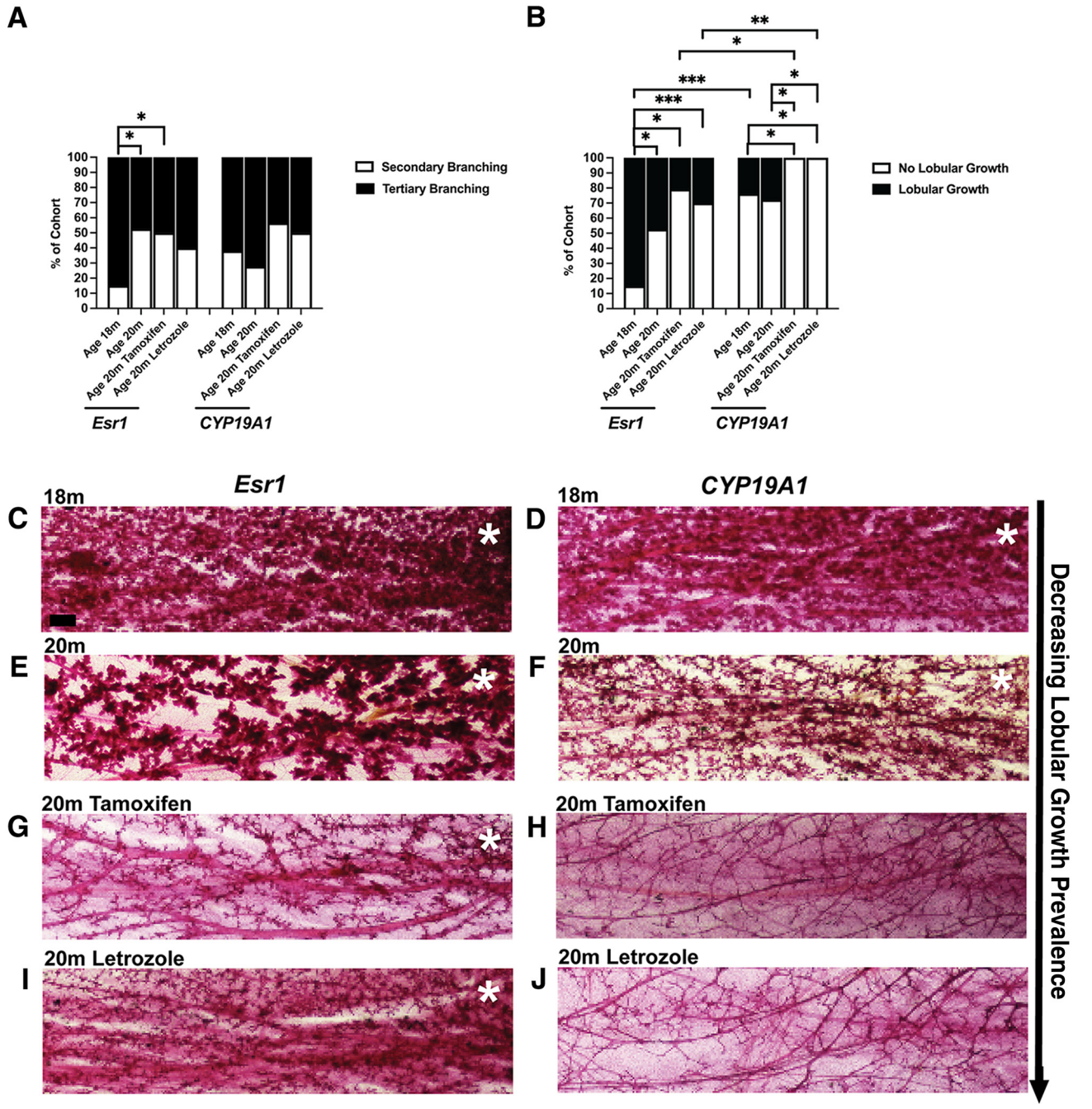

Figure 2 Impact of reproductive senescence and anti-hormonal exposure on patterns of mammary gland branching and lobular growth in mouse estrogen receptor 1 (*Esr1*) and human cytochrome P450 family 19 subfamily A member 1 (aromatase; *CYP19A1*) mice. **A:** Bar graphs illustrating percentage of *Esr1* and *CYP19A1* mice with secondary and tertiary branching in each cohort. *Esr1*: age 18 months (m) $n = 20$; age 20m $n = 19$; age 20m tamoxifen $n = 24$; age 20m letrozole $n = 20$. *CYP19A1*: age 18m $n = 21$; age 20m $n = 18$; age 20m tamoxifen $n = 23$; age 20m letrozole $n = 24$. **B:** Bar graphs illustrating percentage of *Esr1* and *CYP19A1* mice with and without lobular growth in each cohort. *Esr1*: age 18m $n = 20$; age 20m $n = 19$; age 20m tamoxifen $n = 24$; age 20m letrozole $n = 20$. *CYP19A1*: age 18m $n = 21$; age 20m $n = 18$; age 20m tamoxifen $n = 23$; age 20m letrozole $n = 24$. **C**–**J:** Representative mammary gland whole mounts of 18-month–old *Esr1* (**C**) and *CYP19A1* (**D**) mice, 20-month–old *Esr1* (**E**) and *CYP19A1* (**F**) mice, tamoxifen-exposed 20-month–old *Esr1* (**G**) and *CYP19A1* (**H**) mice, and letrozole-exposed *Esr1* (**I**) and *CYP19A1* (**J**) mice, with **right-hand arrow** indicating generally decreasing lobular growth prevalence with age and anti-hormonal exposure. All images scaled identically. **White asterisks** indicate presence of lobular growth to varying degrees in different cohorts. $^{*}P < 0.05$, $^{**}P < 0.01$, and $^{***}P < 0.001$ (Fisher exact test, two sided, GraphPad Prism version 9.3.1). Scale bar = 1000 μm (**C**–**J**). Original magnification, ×0.5 (**C**–**J**).

models was the generally higher prevalence of lobular growth in the *Esr1* mice across different ages and treatment groups, with reductions in prevalence with age and anti-hormonal exposure (Figure 2, C–J). Transgene expression was retained in all cohorts despite reductions in epithelial cell content with age, and anti-hormonal treatment was validated by RT-PCR (Supplemental Figure S1A).

Esr1 Mice Show Significantly More Abnormal Mammary Pathology than *CYP19A1* Mice during Reproductive Senescence

H&E-stained slides of mammary gland tissue were used to assess cellularity and prevalence of preneoplasia (ductal hyperplasia, lobular hyperplasia, ductal carcinoma *in situ*, and adenosis) and invasive cancer (adenosquamous carcinoma and adenocarcinoma) during reproductive senescence and with anti-hormonal exposure. Mammary gland whole mounts were used to score the presence or absence of HANs. Relative cellularity decreased with tamoxifen and letrozole in both models but remained significantly higher in *Esr1* compared with *CYP19A1* mice with tamoxifen exposure (Figure 3A). The percentage of mice with HANs was higher in 18-month–old *Esr1*

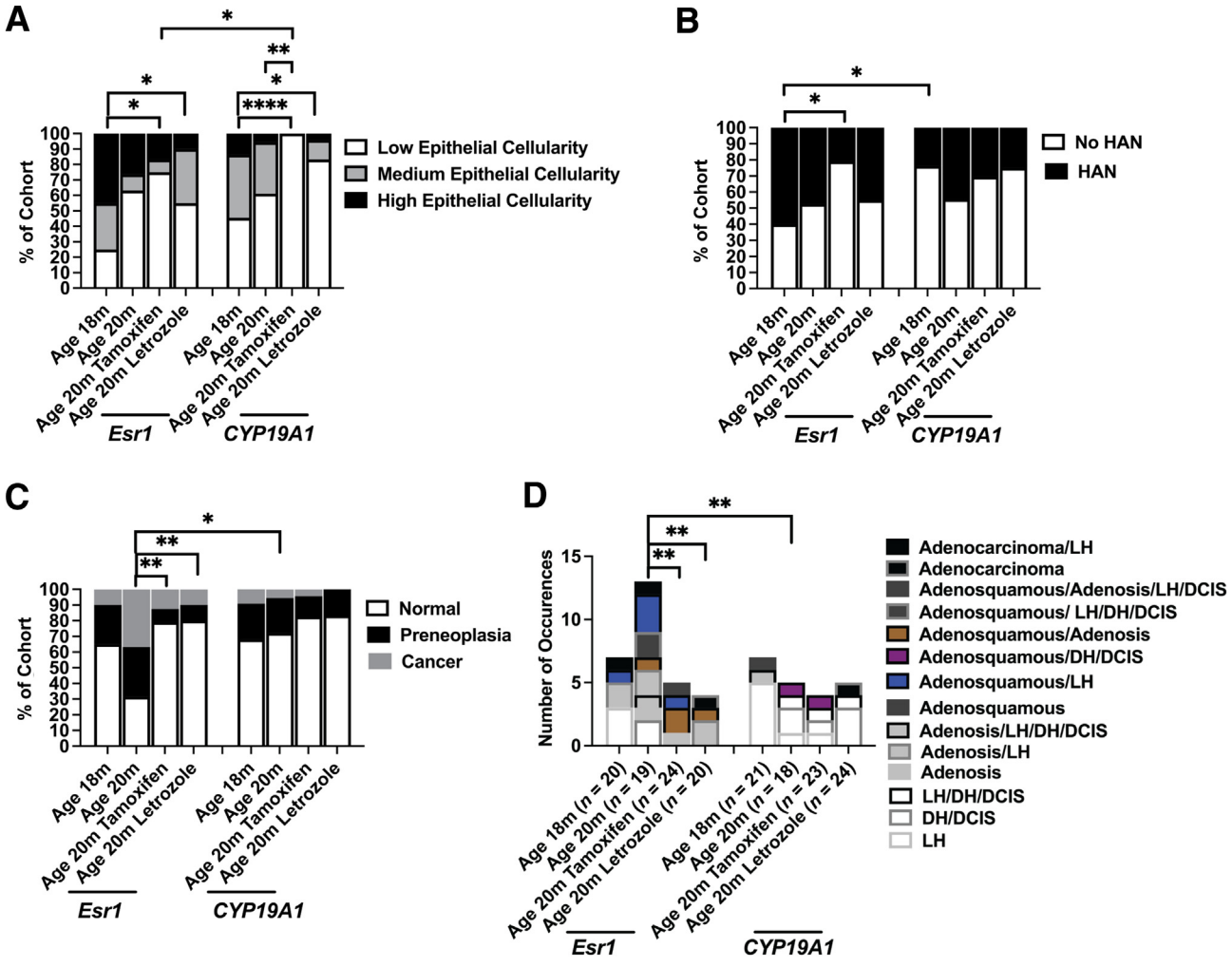

Figure 3 Effect of reproductive senescence and anti-hormonal exposure on mammary gland cellularity, preneoplasia, and cancer in *Esr1* and *CYP19A1* mice. **A:** Bar graphs illustrate percentage of mice with low, medium, or high epithelial cellularity in *Esr1* and *CYP19A1* cohorts. *Esr1*: age 18 months (m) $n = 20$; age 20m $n = 19$; age 20m tamoxifen $n = 24$; age 20m letrozole $n = 20$. *CYP19A1*: age 18m $n = 22$; age 20m $n = 18$; age 20m tamoxifen $n = 23$; age 20m letrozole $n = 24$. *P* values determined by Fisher exact test, Freeman-Halton extension (*http://vassarstats.net/fisher2x3.html*, last accessed August 7, 2022). **B:** Bar graphs illustrate percentage of mice with at least one hyperplastic alveolar nodule (HAN) detected in *Esr1* and *CYP19A1* cohorts. *Esr1*: age 18m $n = 20$; age 20m $n = 19$; age 20m tamoxifen $n = 24$; age 20m letrozole $n = 20$. *CYP19A1*: age 18m $n = 21$; age 20m $n = 18$; age 20m tamoxifen $n = 23$; age 20m letrozole $n = 24$. *P* values determined by Fisher exact test, two sided, GraphPad Prism version 9.3.1. **C:** Bar graphs illustrate percentage of *Esr1* and *CYP19A1* mice with completely normal versus preneoplastic versus cancer findings. *Esr1*: age 18m $n = 20$; age 20m $n = 19$; age 20m tamoxifen $n = 24$; age 20m letrozole $n = 20$. *CYP19A1*: age 18m $n = 22$; age 20m $n = 18$; age 20m tamoxifen $n = 23$; age 20m letrozole $n = 24$. *P* values determined by Fisher exact test, Freeman-Halton extension (*http://vassarstats.net/fisher2x3.html*, last accessed August 7, 2022). **D:** Bar graphs illustrating numbers of combinations of preneoplasia and cancer found in *Esr1* and *CYP19A1* mice. Total number of mice in each cohort listed on *x* axis. *P* values determined by Fisher exact test, two sided, GraphPad Prism version 9.3.1, number of mice with preneoplasia/cancer versus those with only normal findings. $*P < 0.05$, $**P < 0.01$, and $****P < 0.0001$. DCIS, ductal carcinoma *in situ*; DH, ductal hyperplasia; LH, lobular hyperplasia.

compared with that in *CYP19A1* mice (Figure 3B). At age 20 months, *Esr1* mice demonstrated significantly more preneoplasia and cancer than *CYP19A1* mice, which was abrogated by both tamoxifen and letrozole exposure (Figure 3, C and D). ER immunohistochemistry was used to assess patterns of nuclear-localized ER staining in normal, preneoplastic, and cancerous mammary tissue. Patterns of ER staining in normal-appearing ducts were not significantly altered by age or anti-hormonal exposure (Figure 4, A–C, and Supplemental Figure S1, B–F). Ductal and lobular hyperplasias showed higher percentages of ER^+ cells compared with normal ducts (Figure 4, D–G) without significant differences between the models. Ductal carcinoma *in situ* lesions were most commonly ER^+ (Figure 4, H and I), but an ER^- ductal carcinoma *in situ* lesion was identified in a *CYP19A1* mouse (Figure 4J). Adenosis and adenosquamous lesions were ER^+ in both models (Figure 4, K–P). One ER^- adenocarcinoma was found in an *Esr1* mouse (Figure 4Q). The other adenocarcinomas were ER^+ (Figure 4R). In summary, *Esr1* mice showed higher prevalence and more advanced mammary pathology compared with *CYP19A1* mice; however, the disease itself was histologically similar between models. An important finding was the relatively high prevalence of ER^+ disease in the *Esr1* and *CYP19A1* mice during reproductive senescence with initiation of transgene expression at age 12 months that could be reduced by exposure to tamoxifen or letrozole.

Expression of Cell Proliferation Genes Is Significantly Higher in *Esr1* Mice during Reproductive Senescence but Is Down-Regulated with Anti-Hormonal Exposure

RNA-sequencing analyses were used to explore transcriptional changes induced by *Esr1* compared with *CYP19A1* expression during reproductive senescence and with tamoxifen and letrozole exposure. Significantly differentially expressed protein-coding genes (DEGs) were compared for each end point/treatment condition between the two models and subjected to Gene Set Enrichment Analyses. Numbers of DEGs and top three gene enrichment sets for each comparison were determined (Figure 5, A–L). The largest numbers of DEGs between the models were found at age 20 months in the absence of anti-hormonal exposure, with significant enrichment in HALLMARK_G2M_CHECKPOINT, HALLMARK_E2F_TARGETS, and HALLMARK_MITOTIC_SPINDLE in the DEGs expressed at significantly higher levels in the *Esr1* mice (Figure 5, D–F). Individual significantly differentially expressed genes identified for each enrichment group with fold change in expression levels between genotypes

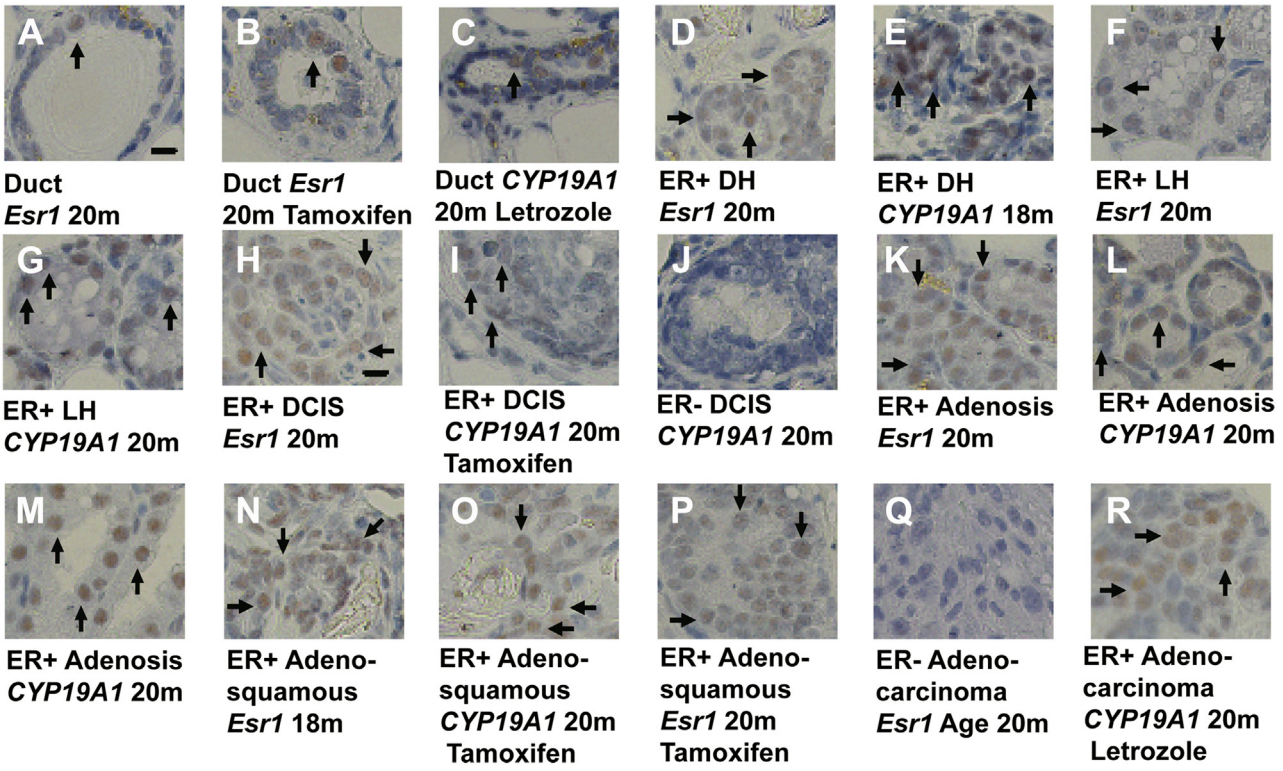

Figure 4 Comparison of histology and estrogen receptor α (ER) immunohistochemistry in mouse estrogen receptor 1 (*Esr1*) and human cytochrome P450 family 19 subfamily A member 1 (aromatase; *CYP19A1*) mice. Representative images of ER immunohistochemistry of normal ducts (**A**–**C**), ductal hyperplasia (DH; **D** and **E**), lobular hyperplasia (LH; **F** and **G**), ductal carcinoma *in situ* (DCIS; **H**–**J**), adenosis (**K**–**M**), adenosquamous cancers (**N**–**P**), and adenocarcinomas (**Q** and **R**). For comparison, representative images of ER immunohistochemistry of normal ducts from *CYP19A1* 20-month–old, tamoxifen-exposed *CYP19A1* 20-month–old, and letrozole-exposed *Esr1* mice shown in Supplemental Figure S1. **Black arrows** indicate representative cells with nuclear-localized ER staining. Scale bar = 10 μm (**A**–**R**).

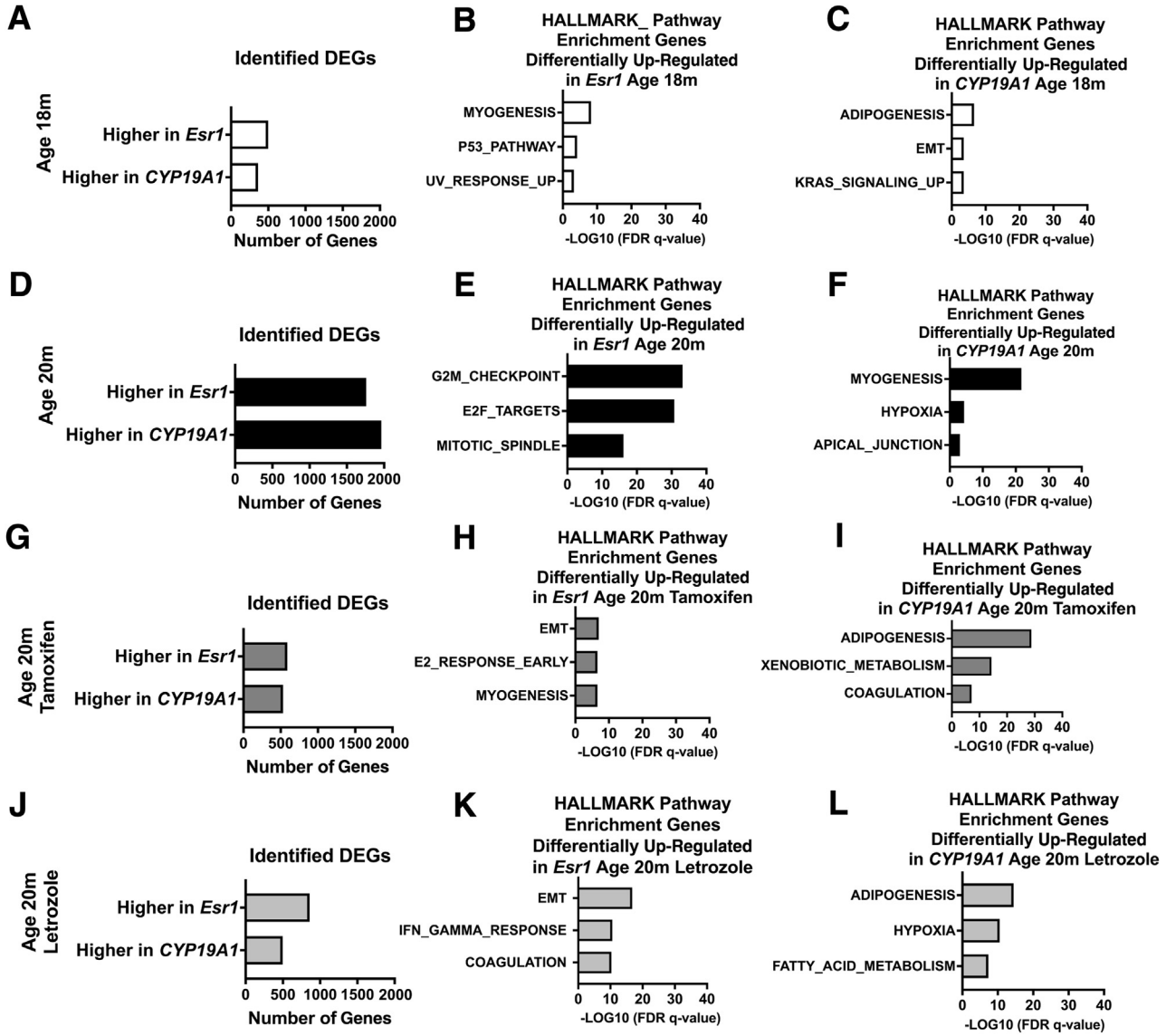

Figure 5 RNA-sequencing analyses indicating mouse estrogen receptor 1 (*Esr1*) and human cytochrome P450 family 19 subfamily A member 1 (aromatase; *CYP19A1*) mice with the highest numbers of differentially expressed genes (DEGs) at age 20 months (m), and *Esr1* mice with significant enrichment in HALLMARK gene sets related to cell cycle progression. **A:** Bar graphs presenting numbers of statistically significantly differentially expressed protein-coding genes between *Esr1* and *CYP19A1* mice at age 18m. *P*-value adjusted (*P*adj) < 0.05 (DESeq2). **B:** Bar graphs showing three HALLMARK gene sets with smallest −LOG10 false discovery rate (FDR) q-values following Gene Set Enrichment Analysis (GSEA) of protein-coding genes significantly up-regulated in *Esr1* mice at age 18m. **C:** Bar graphs showing three HALLMARK gene sets with smallest −LOG10 FDR q-values following GSEA of protein-coding genes significantly up-regulated in *CYP19A1* mice at age 18m. **D:** Bar graphs presenting numbers of statistically significantly differentially expressed protein-coding genes between *Esr1* and *CYP19A1* mice at age 20m. *P*adj < 0.05 (DESeq2). **E:** Bar graphs showing three HALLMARK gene sets with smallest −LOG10 FDR q-values following GSEA of protein-coding genes significantly up-regulated in *Esr1* mice at age 20m. **F:** Bar graphs showing three HALLMARK gene sets with smallest −LOG10 FDR q-values following GSEA of protein-coding genes significantly up-regulated in *CYP19A1* mice at age 20m. **G:** Bar graphs presenting numbers of statistically significantly differentially expressed protein-coding genes between *Esr1* and *CYP19A1* mice at age 20m following 2 months tamoxifen exposure. *P*adj < 0.05 (DESeq2). **H:** Bar graphs showing three HALLMARK gene sets with smallest −LOG10 FDR q-values following GSEA of protein-coding genes significantly up-regulated in *Esr1* mice at age 20m following 2 months tamoxifen exposure. **I:** Bar graphs showing three HALLMARK gene sets with smallest −LOG10 FDR q-values following GSEA of protein-coding genes significantly up-regulated in *CYP19A1* mice at age 20m following 2 months tamoxifen exposure. **J:** Bar graphs presenting numbers of statistically significantly differentially expressed protein-coding genes between *Esr1* and *CYP19A1* mice at age 20m following 2 months letrozole exposure. *P*adj < 0.05 (DESeq2). **K:** Bar graphs showing three HALLMARK gene sets with smallest −LOG10 FDR q-values following GSEA of protein-coding genes significantly up-regulated in *Esr1* mice at age 20m following 2 months tamoxifen exposure. **L:** Bar graphs showing three HALLMARK gene sets with smallest −LOG10 FDR q-values following GSEA of protein-coding genes significantly up-regulated in *CYP19A1* mice at age 20m following 2 months tamoxifen exposure. $n = 3$ mice per cohort (**A**–**L**). E2, estrogen; E2F, E2 transcription factor; EMT, epithelial-mesenchymal transition; IFN, interferon; KRAS, Kirsten rat sarcoma viral oncogene homolog.

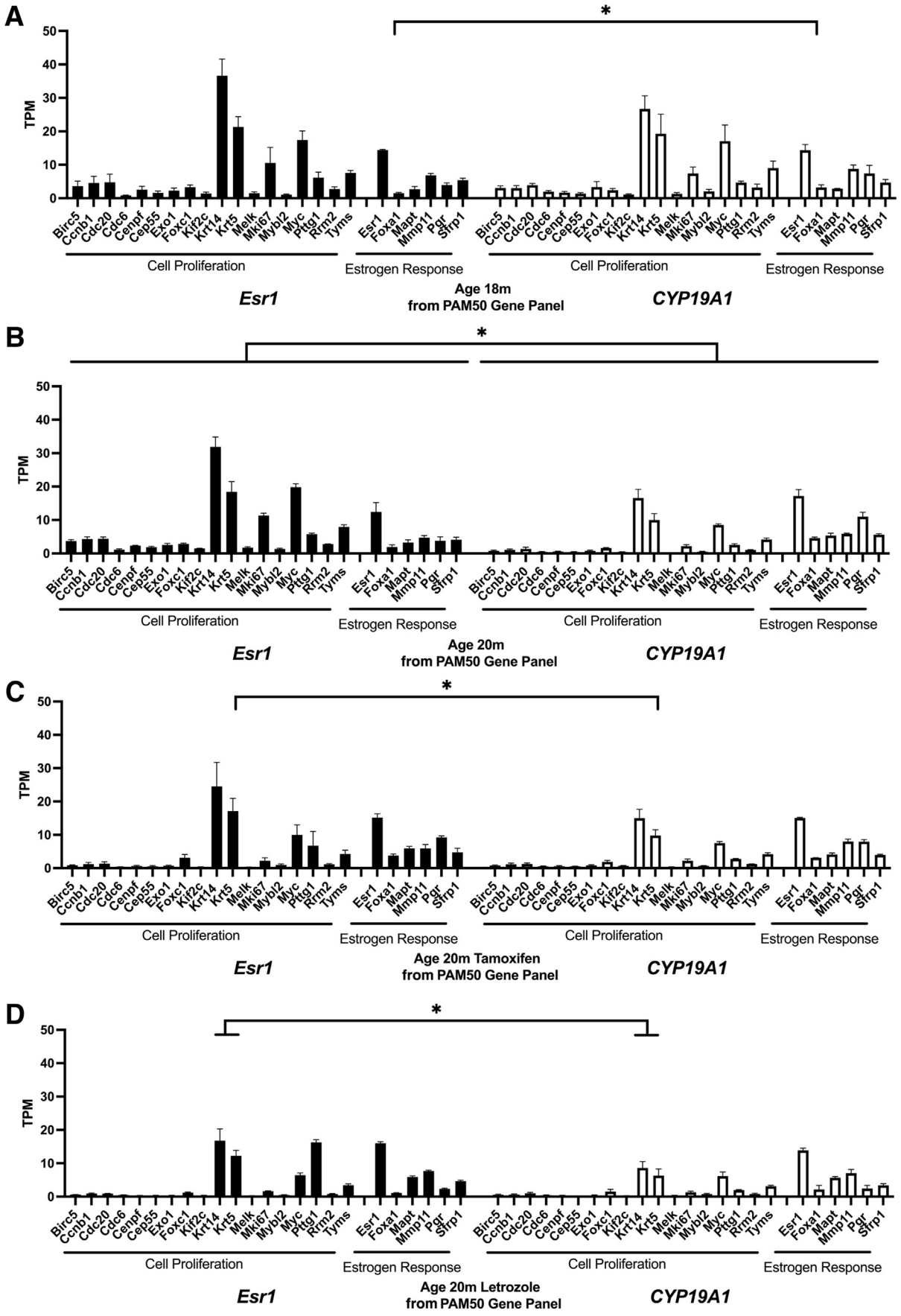
A
B
C
D
TPM
Cell Proliferation
Estrogen Response
Esr1
CYP19A1
Age 18m
from PAM50 Gene Panel
Age 20m
from PAM50 Gene Panel
Age 20m Tamoxifen
from PAM50 Gene Panel
Age 20m Letrozole
from PAM50 Gene Panel

and individual level of statistical significance are presented in Supplemental Table S1. To explore the relevancy of the pathologic and molecular differences observed in the *Esr1* and *CYP19A1* models with human breast cancer, identified DEGs were compared with the human PAM50 gene panel to determine whether any of the PAM50 panel genes were differentially expressed between *Esr1* and *CYP19A1* mice (Figure 6). The specific intent was to determine whether there was a correlation between the higher rate of abnormal pathology in the *Esr1* mice with higher expression of any PAM50 genes. Expression levels of genes from the PAM50 profile were largely comparable between models at age 18 months (Figure 6A). However, at age 20 months, 18 cell proliferation–related genes were expressed at significantly higher levels in *Esr1* compared with *CYP19A1* mice (Figure 6B). Six estrogen response–related genes from the PAM50 gene panel were identified as significantly higher expressed in the *CYP19A1* mice compared with the *Esr1* mice at age 20 months (Figure 6B). Expression levels following tamoxifen (Figure 6C) and letrozole (Figure 6D) exposure were lower and largely comparable between genotypes. Statistical analyses of relative expression levels within genotypes across age and exposure groups show how exposure to tamoxifen and letrozole was associated with significant down-regulation of cell proliferation genes in *Esr1* mice (Supplemental Figure S2), with *Foxa1*, *Pgr*, and *Sfrp1* being significantly down-regulated in the *CYP19A1* mice (Supplemental Figure S3). Relative expression levels of luminal (*Krt7*, *Krt8*, *Krt18*, and *Krt19*) and basal (*Krt5* and *Krt14*) cytokeratins were compared across genotypes and exposure groups for a general assessment of mammary epithelial cell content and relative populations of luminal and basal mammary epithelial cells in the different samples (Supplemental Figure S4). Luminal cytokeratins were expressed at the same or higher levels in samples from *CYP19A1* mice compared with samples from *Esr1* mice of the same age and/or exposure group, suggesting mammary epithelial cell content in the samples used for RNA sequencing was reasonably comparable between samples. Significantly higher levels of *Krt5* and *Krt14*, found in *Esr1* mice, are consistent with possible differences in mammary epithelial cell populations as well as being compatible with the higher proliferation rates at age 20 months in these mice. Significantly lower luminal *Krt* expression levels following letrozole were found in both *Esr1* and *CYP19A1* mice. The analysis of the PAM50 panel highlighted the impact of *Esr1* and *CYP19A1* overexpression on cell proliferation and estrogen response genes. Both models develop ER^+ pathology and express *Esr1* (Figures 4 and 6). To explore expression of previously reported genes mediating genomic versus nongenomic mechanisms of estrogen receptor–mediated cell proliferation,[7–11] expression patterns of well-established seven genes linked to genomic signaling (Supplemental Figure S5) and eight genes linked to nongenomic signaling (Supplemental Figure S6) were investigated. All 15 genes were expressed across all cohorts. There was evidence of down-regulation for four of the seven genomic signaling genes with anti-hormonal exposure in whole mammary tissue in the mouse models as these networks are consistent with activity at the transcriptional level. Nongenomic mechanisms are largely mediated by protein-protein interactions and were not expected to show major transcriptional changes.

Aberrant Pregnancy Development-Related Gene Signature Identified in *Esr1* Mice

Inspection of the cell proliferation– and estrogen response–related genes expressed at significantly higher levels in *Esr1* mice that were coincidently members of the PAM50 gene panel revealed nine genes that are known to be developmentally regulated during pregnancy in the mammary gland (Figure 7A). The six cell proliferation–related genes were all up-regulated mid pregnancy (day 13, mouse pregnancy, GSE70440, *https://www.ncbi.nlm.nih.gov/geo/query/acc.cgi?acc=GSE70440*, last accessed September 17, 2022) with persistent higher expression levels through late pregnancy (day 18, mouse pregnancy, GSE70440, *https://www.ncbi.nlm.nih.gov/geo/query/acc.cgi?acc=GSE70440*, last accessed September 17, 2022). The three estrogen response–related genes were all down-regulated with late pregnancy. A heat map of the *Esr1* and *CYP19A1* mice focusing only on these nine genes demonstrated aberrant day 13 to 18 pregnancy-like patterns of expression in 18- and 20-month–old *Esr1* mice and 18-month–old *CYP19A1* mice with anti-hormonal exposure generally associated with the lowest expression levels (Figure 7B). To test whether other pregnancy development-related genes would show similar patterns, 34 additional genes known to be regulated during pregnancy were arrayed in heat maps for both the normal

Figure 6 Significant differences in expression levels of cell proliferation and estrogen response genes between mouse estrogen receptor 1 (*Esr1*) and human cytochrome P450 family 19 subfamily A member 1 (aromatase; *CYP19A1*) mice at age 20 months (m) were generally resolved by anti-hormonal exposure. Bar graphs showing comparative expression levels of cell proliferation and estrogen signaling genes from the human Prediction Analysis of Microarray 50 (PAM50) prognostic gene panel for estrogen receptor α–positive (ER^+) breast cancer in *Esr1* and *CYP19A1* mice at age 18m (**A**), age 20m (**B**), age 20m following 2 months of tamoxifen exposure (**C**), and age 20m following 2 months of letrozole exposure (**D**). Data are given as means ± SEM (**A**–**D**). $n = 3$ mice per cohort (**A**–**D**). **P*-value adjusted < 0.05 (DESeq2). *Birc5*, baculoviral IAP repeat containing 5; *Ccnb1*, cyclin B1; *Cdc20*, cell division cycle 20; *Cdc6*, cell division cycle 6; *Cenpf*, centromere protein F; *Cep55*, centrosomal protein 55; *Exo1*, exonuclease 1; *Foxa1*, forkhead box A1; *Foxc1*, forkhead box C1; *Kif2c*, kinesin family member 2; *Krt14*, keratin 14; *Krt5*, keratin 5; *Mapt*, microtubule-associated protein tau; *Melk*, maternal embryonic leucine zipper kinase; *Mki67*, marker of proliferation Ki-67; *Mmp11*, matrix metallopeptidase 11; *Mybl2*, MYB proto-oncogene like 2; *Myc*, MYC proto-oncogene, BHLH transcription factor; *Pgr*, progesterone receptor; *Pttg1*, PTTG1 regulator of sister chromatid separation, securin; *Rrm2*, ribonucleotide reductase regulatory subunit M2; *Sfrp1*, secreted frizzled related protein 1; TPM, transcripts per million; *Tyms*, thymidylate synthetase.

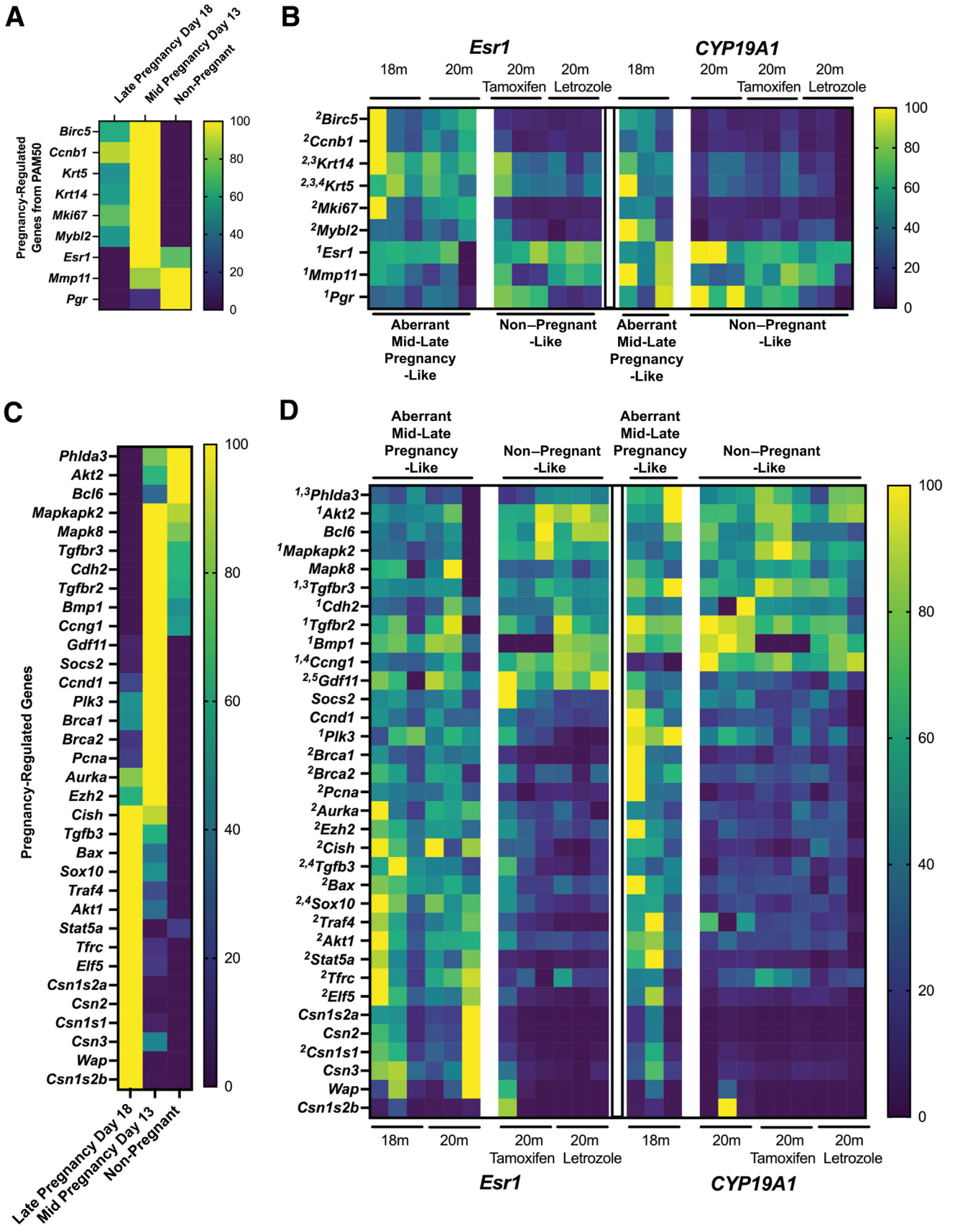
A
Late Pregnancy Day 18
Mid Pregnancy Day 13
Non-Pregnant
Pregnancy-Regulated Genes from PAM50
Birc5
Ccnb1
Krt5
Krt14
Mki67
Mybl2
Esr1
Mmp11
Pgr
100
80
60
40
20
0
B
Esr1
CYP19A1
18m
20m
20m Tamoxifen
20m Letrozole
18m
20m
20m Tamoxifen
20m Letrozole
2Birc5
2Ccnb1
2,3Krt14
2,3,4Krt5
2Mki67
2Mybl2
1Esr1
1Mmp11
1Pgr
Aberrant Mid-Late Pregnancy -Like
Non–Pregnant -Like
Aberrant Mid-Late Pregnancy -Like
Non–Pregnant -Like
C
Pregnancy-Regulated Genes
Phlda3
Akt2
Bcl6
Mapkapk2
Mapk8
Tgfbr3
Cdh2
Tgfbr2
Bmp1
Ccng1
Gdf11
Socs2
Ccnd1
Plk3
Brca1
Brca2
Pcna
Aurka
Ezh2
Cish
Tgfb3
Bax
Sox10
Traf4
Akt1
Stat5a
Tfrc
Elf5
Csn1s2a
Csn2
Csn1s1
Csn3
Wap
Csn1s2b
Late Pregnancy Day 18
Mid Pregnancy Day 13
Non-Pregnant
D
Aberrant Mid-Late Pregnancy -Like
Non–Pregnant -Like
Aberrant Mid-Late Pregnancy -Like
Non–Pregnant -Like
1,3Phlda3
1Akt2
Bcl6
1Mapkapk2
Mapk8
1,3Tgfbr3
1Cdh2
1Tgfbr2
1Bmp1
1,4Ccng1
2,5Gdf11
Socs2
Ccnd1
1Plk3
2Brca1
2Brca2
2Pcna
2Aurka
2Ezh2
2Cish
2,4Tgfb3
2Bax
2,4Sox10
2Traf4
2Akt1
2Stat5a
2Tfrc
2Elf5
Csn1s2a
Csn2
2Csn1s1
Csn3
Wap
Csn1s2b
18m
20m
20m Tamoxifen
20m Letrozole
18m
20m
20m Tamoxifen
20m Letrozole
Esr1
CYP19A1

pregnancy reference data (Figure 7C) and the experimental cohorts (Figure 7D). The pattern persisted with genes expressed at higher levels mid and late pregnancy being higher expressed in *CYP19A1* mice at age 18 months and *Esr1* mice at ages 18 and 20 months. Of the 34 known pregnancy-related genes, 25 of them were identified as significant DEGs between the two models at 18 and/or 20 months of age. Taken together, the study of pregnancy-related gene expression in the two models revealed that *Esr1* mice exhibited an abnormal mid-late pregnancy-like pattern of gene expression during reproductive senescence at age 20 months compared with *CYP19A1* mice that more closely resemble normal non-pregnant patterns of gene expression at that end point.

Pregnancy-Like Morphology Accompanies Pregnancy-Like Gene Expression with Resolution by Tamoxifen or Letrozole Exposure

Given the significant differences in mid-late pregnancy-related gene expression between the two models, the next question was whether mammary gland whole mount findings reminiscent of pregnancy would be found at higher prevalence in *Esr1* compared with *CYP19A1* mice. Mammary gland whole mounts were assessed for the appearance of dense uniform alveolar-like growth normally found during late pregnancy in mice as well as overall mammary gland density. Significantly higher prevalence of dense uniform alveolar growth and increased mammary density were identified in *Esr1* compared with *CYP19A1* mice at age 18 months (Figure 8, A and B). Tamoxifen exposure was associated with significant reductions in both alveolar-like growth and density, consistent with the significant reductions in tertiary branching and lobular growth, cellularity, HANs, preneoplasia, and cancer documented (Figures 2, A and B, and 3). This was a provocative finding because 12-month–old *Esr1* mice experiencing transgene overexpression since birth demonstrate tamoxifen resistance linked to increased gene expression of interferon-γ–related genes.[19] To test whether sensitivity to tamoxifen in the *Esr1* mice undergoing reproductive senescence was associated with decreased expression levels of interferon-γ genes, relative gene expression levels were compared with previously published reference data (GSE63857, *https://www.ncbi.nlm.nih.gov/geo/query/acc.cgi?acc=GSE63857*, last accessed September 17, 2022) after renormalization with the current RNA-sequencing data set. For most genes identified as DEGs between *Esr1* and *CYP19A1* mice at age 12 months, expression was decreased in the *Esr1* mice at ages 18 and 20 months (Figure 8C), consistent with a role for these genes in mediating tamoxifen resistance.

Discussion

A fundamental question in biology and medicine and especially in age-associated diseases, such as breast cancer, is how aging influences disease presentation.[74] In women, age-specific rates of ER^+ breast cancers increase with age following menopause.[75] Overexpressions of *Esr1* and *CYP19A1* in breast tissue are two distinct perturbations of estrogen pathway signaling found in women with breast cancer,[5,6,76–79] that are modeled in the mice presented herein.[19,34,80] This study demonstrated that disease presentation in the *Esr1* and *CYP19A1* mice is impacted by age with accompanying reproductive senescence. Although pre–reproductive senescent 12-month–old mice show

Figure 7 Mouse estrogen receptor 1 (*Esr1*) overexpression associated with abnormal expression patterns of pregnancy-related genes. **A:** Heat map showing relative expression levels of nine pregnancy-regulated genes identified as differentially expressed between *Esr1* and human cytochrome P450 family 19 subfamily A member 1 (aromatase; *CYP19A1*) mice age 20 months (m) that are also members of the human Prediction Analysis of Microarray 50 (PAM50) prognostic gene panel for estrogen receptor α–positive (ER^+) breast cancer at late pregnancy (day 18), mid-pregnancy (day 13), and in non-pregnant mice (downloaded data from 2-month–old mice: GSE70440, *https://www.ncbi.nlm.nih.gov/geo/query/acc.cgi?acc=GSE70440*, last accessed September 17, 2022). **B:** Heat map highlighting end points with aberrant pregnancy-like and non–pregnant-related expression patterns of the nine pregnancy-related genes across all four end points in the *Esr1* and *CYP19A1* mice. [1]Genes expressed at significantly higher levels in *CYP19A1* mice age 20m: *Esr1*, matrix metallopeptidase 11 (*Mmp11*), and progesterone receptor (*Pgr*). [2]Genes expressed at significantly higher levels in *Esr1* mice age 20m: baculoviral IAP repeat containing 5 (*Birc5*), cyclin B1 (*Ccnb1*), keratin 14 (*Krt14*), keratin 5 (*Krt5*), marker of proliferation Ki-67 (*Mki67*), and MYB proto-oncogene like 2 (*Mybl2*). [3]*Krt14*, *Krt5*, *P*-value adjusted (*P*adj) < 0.05, DESeq2, higher *Esr1* age 20m with 2 months letrozole exposure. [4]*Krt5*, *P*adj < 0.05, DESeq2, higher *Esr1* age 20m with 2 months tamoxifen exposure. **C:** Heat map illustrating relative expression levels of an additional 34 pregnancy-regulated genes at late pregnancy (day 18), mid-pregnancy (day 13), and in non-pregnant mice. **D:** Heat map highlighting end points with aberrant pregnancy-like and non–pregnant-related expression patterns of the 34 additional pregnancy-related genes across all four end points in the *Esr1* and *CYP19A1* mice. [1]Genes expressed at significantly higher levels in *CYP19A1* mice age 20m: Pleckstrin homology-like domain family A member 3 (*Phlda3*), AKT serine/threonine kinase 2 (*Akt2*), mitogen-activated protein kinase activated protein kinase 2 (*Mapkapk2*), transforming growth factor-β receptor 3 (*Tgfbr3*), cadherin 2 (*Cdh2*), transforming growth factor-β receptor 2 (*Tgfbr2*), bone morphogenetic protein 1 (*Bmp1*), cyclin G1 (*Ccng1*), and Polo-like kinase 3 (*Plk3*), *P*adj < 0.05, DESeq2. [2]Genes expressed at significantly higher levels in *Esr1* mice age 20m: growth differentiation factor 11 (*Gdf11*), BRCA1 DNA repair associated (*Brca1*), BRCA2 DNA repair associated (*Brca2*), proliferating cell nuclear antigen (*Pcna*), Aurora kinase A (*Aurka*), enhancer of zeste 2 polycomb repressive complex 2 subunit (*Ezh2*), cytokine-inducible SH2 containing protein (*Cish*), *Tgfb3*, BCL2-associated X, apoptosis regulator (*Bax*), SRY-box transcription factor 10 (*Sox10*), tumor necrosis factor receptor-associated factor 4 (*Traf4*), AKT serine/threonine kinase 1 (*Akt1*), *Stat5a*, transferrin receptor (*Tfrc*), E74-like ETS transcription factor 5 (*Elf5*), and casein α S1 (*Csn1s1*), *P*adj < 0.05, DESeq2. [3]*Phlda3*, *Tgfbr3* *P*adj < 0.05, DESeq2, higher *CYP19A1* age 18m. [4]*Tgfb3*, *Sox10*, *Ccng1* *P*adj < 0.05, DESeq2, higher *Esr1* age 18m. [5]*Gdf11* *P*adj < 0.05, DESeq2, higher *Esr1* age 20m with both 2 months exposure to tamoxifen and letrozole. Yellow indicates highest expression level, and dark blue indicates lowest expression level, for each gene. Relative expression levels shown for unique individual samples. $n = 3$ for each cohort (**B** and **D**). *Bcl6*, BCL6 transcription repressor; *Ccnd1*, cyclin D1; *Csn1s2a*, casein α s2-like A; *Csn1s2b*, casein α s2-like B; *Csn2*, casein β; *Csn3*, casein κ; *Mapk8*, mitogen-activated protein kinase 8; *Socs2*, suppressor of cytokine signaling 2; *Wap*, whey acidic protein.

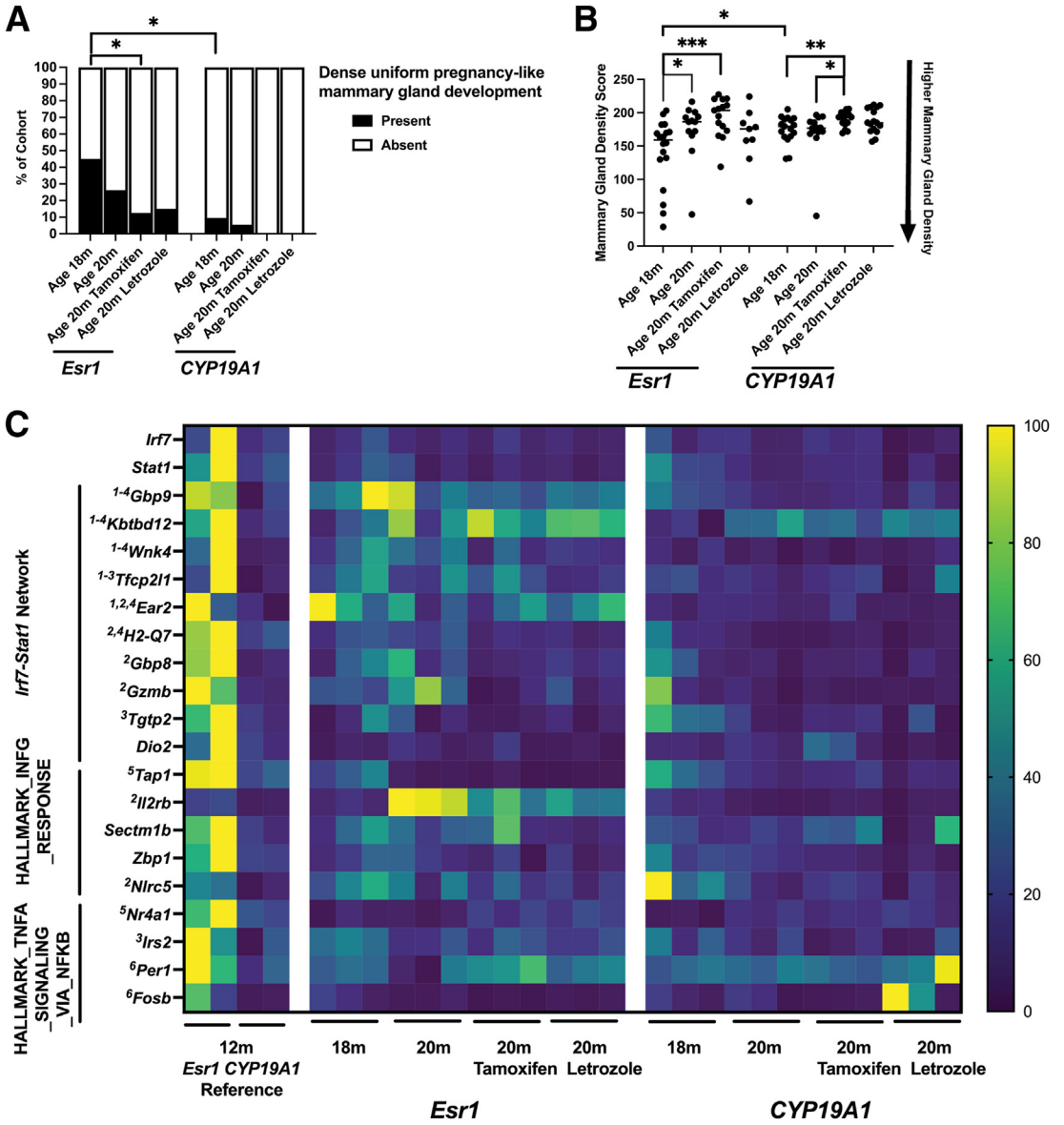

Figure 8 Higher prevalence of dense uniform pregnancy-like alveolar growth and increased overall mammary gland density in mouse estrogen receptor 1 (*Esr1*) mice is resolved by tamoxifen exposure. **A:** Bar graphs illustrate percentage of mice with dense uniform pregnancy-like alveolar development in *Esr1* and human cytochrome P450 family 19 subfamily A member 1 (aromatase; *CYP19A1*) cohorts. *Esr1*: age 18 months (m) $n = 20$; age 20m $n = 19$; age 20m tamoxifen $n = 24$; age 20m letrozole $n = 20$. *CYP19A1*: age 18m $n = 21$; age 20m $n = 18$; age 20m tamoxifen $n = 23$; age 20m letrozole $n = 24$. *P* values determined by Fisher exact test, two sided, GraphPad Prism version 9.3.1. **B:** Scatterplots illustrate distribution of relative mean mammary gland density scores in each cohort of *Esr1* and *CYP19A1* mice. *Esr1*: age 18m $n = 18$; age 20m $n = 13$; age 20m tamoxifen $n = 15$; age 20m letrozole $n = 9$. *CYP19A1*: age 18m $n = 17$; age 20m $n = 14$; age 20m tamoxifen $n = 16$; age 20m letrozole $n = 16$. Median indicated. *P* values determined by *U*-test, two tailed, GraphPad Prism version 9.3.1. **Black arrow** indicates that lower mammary gland density scores, which are based on pixel intensity readings of mammary gland whole mount images, correlate with higher mammary gland density. **C:** Heat map illustrating expression patterns of immune-related genes significantly differentially expressed between *Esr1* and *CYP19A1* mice at 12 months with transgene expression from birth [*P*-value adjusted (*P*adj) < 0.05, DESeq2] versus 18- and 20-month—old cohorts with transgene expression initiated at age 12 months. Differentially expressed genes (DEGs; *P*adj < 0.05, DESeq2) higher in *Esr1* compared with *CYP19A1* mice at age 18 m[1], age 20 m[2], age 20m following 2 months tamoxifen exposure[3], and age 20m following 2 months of letrozole exposure[4]. DEGs (*P*adj < 0.05, DESeq2) higher in *CYP19A1* compared with *Esr1* mice at age 20 m[5] and age 20m following 2 months of letrozole exposure[6]. Yellow indicates highest expression level, and dark blue indicates lowest expression level, for each gene. Relative expression levels shown for unique individual samples. 12m cohorts: $n = 2$. 18m and 20m cohorts: $n = 3$. $^*P < 0.05$, $^{**}P < 0.01$, and $^{***}P < 0.001$. *Dio2*, iodothyronine deiodinase; *Ear2*, eosinophil-associated, ribonuclease A family, member 2; *Fosb*, FosB proto-oncogene, AP-1 transcription factor subunit; *Gbp8*, guanylate-binding protein 8; *Gbp9*, guanylate-binding protein 9; *Gzmb*, granzyme B; *H2*-Q7, histocompatibility 2, Q region locus 7; IFNG, interferon-γ; *Il2rb*, IL-2 receptor subunit β; Irf7, interferon regulatory factor 7; *Irs2*, insulin receptor substrate 2; *Kbtdb12*, Kelch repeat and BTB domain containing 12; NFKB, NF-κB; *Nlrc5*, NLR family CARD domain-containing 5; *Nr4a1*, nuclear receptor subfamily 4 group A member 1; *Per1*, period circadian regulator 1; *Sectm1b*, secreted and transmembrane protein 1b; *Tap1*, transporter 1, ATP binding cassette subfamily B member; *Tfcp2l1*, transcription factor CP2-like 1; *Tgtp2*, T-cell—specific GTPase 2; TNFA, tumor necrosis factor-α; *Wnk4*, WNK lysine-deficient protein kinase 4; *Zbp1*, Z-DNA binding protein 1.

slightly higher disease rates with *CYP19A1* overexpression compared with *Esr1* overexpression, this was reversed in 20-month–old mice in reproductive senescence, where *Esr1* overexpression was associated with significantly higher disease rates. This higher disease rate was linked to a pattern of higher expression of proliferation-related genes that was maintained through reproductive senescence, even as estrogen-linked ovarian function was lost and there was evidence of mammary gland involution noted by loss of tertiary branching, lobular growth, and overall mammary gland density. This pattern was not seen in the *CYP19A1* mice, showing that ovarian reproductive senescence impacted these two components of the estrogen signaling pathway differently. A possible explanation for the lower rates of cell proliferation and disease in the *CYP19A1* mice could be decreased androgen production, required by aromatase for estrogen production, from the senescent ovaries.[81]

Persistent activity of ER α–driven growth pathways through reproductive senescence maintained an aberrant pregnancy-like proliferative gene expression profile in the *Esr1* mice that correlated with a higher prevalence of preneoplasia and cancer in this model. High-risk breast cells from women with breast cancer can exhibit a similar profile.[28] During normal pregnancy, estrogen signaling pathways initiate a stage of proliferative alveolar morphogenesis that is followed by differentiation into milk-producing cells.[82] Failure of proliferative cells to differentiate is a cancer risk factor, well studied in human papillomavirus–induced cervical carcinogenesis.[83] Pregnancy at younger ages exerts a protective effect on breast cancer generation, but initial pregnancy at older ages is associated with increased breast cancer risk.[84–86] In this study, induction of abnormal levels of *Esr1* was initiated in 12-month–old mice, equivalent to human middle age. The significant amount of preneoplasia and cancer found in both 18- and 20-month–old *Esr1* mice only 6 and 8 months following transgene expression may be attributed to the aging mammary epithelium that the transgene induction was initiated in.

Both tamoxifen and letrozole exposure were effective in reducing prevalence of preneoplasia and cancer. This was an unexpected finding in the *Esr1* mice as they have reproducibly demonstrated tamoxifen resistance linked to the presence of an activated *Irf7-Stat1* network.[19,35,36] The presence of tamoxifen responsiveness demonstrated herein was associated with down-regulation of this network. Similar to this observation, a second immunologic pathway, NF-κB subunit 1 signaling, has been linked to tamoxifen resistance in women[87] and was activated in the younger tamoxifen-resistant *Esr1* mice but down-regulated in the tamoxifen-responsive older mice. Most preneoplastic and cancer disease found in the mice was ER α^+, consistent with its resolution with tamoxifen and letrozole exposure.

In summary, investigation of mammary disease initiated by overexpression of *Esr1* and *CYP19A1* in mid-age mice yielded a series of new observations relevant to human breast cancer. First, *Esr1* overexpression but not *CYP19A1* overexpression was associated with a persistent proliferative response through reproductive senescence. Second, this proliferative response was embedded within an aberrant pregnancy-like gene expression profile and included known prognostic signature genes for human ER^+ breast cancer. Third, aging and entry into reproductive senescence altered tamoxifen responsiveness of the *Esr1* mice. Finally, expansion of mouse model studies of breast cancer generation through natural reproductive senescence yielded new insights into mammary disease induced by *Esr1* and *CYP19A1* overexpression that more closely resembles the natural history of breast carcinogenesis in women, where most of the disease develops with and after menopause.

Acknowledgment

We thank Georgetown University–Lombardi Shared Resources Animal Models, Genomics and Epigenomics, Histopathology and Tissue for contributions to the research.

Author Contributions

P.A.F. conceived the study; P.A.F., W.W., and J.A.F. designed the study; P.A.F., W.W., K.K., B.L.R., V.M., X.Z., and J.A.F. acquired data; P.A.F., K.K., B.L.R., G.K., V.M., and J.A.F. interpreted and analyzed data; P.A.F. and B.L.R. prepared the initial manuscript; P.A.F., W.W., K.K., B.L.R., G.K., V.M., X.Z., and J.A.F. reviewed the manuscript before submission and acceptance of authorship; and P.A.F. secured funding. P.A.F. is the guarantor of this work and, as such, had full access to all of the data in the study and takes responsibility for the integrity of the data and the accuracy of the data analysis.

Supplemental Data

Supplemental material for this article can be found at *http://doi.org/10.1016/j.ajpath.2022.09.007*.

References

1. Trapani D, Ginsburg O, Fadelu T, Lin NU, Hassett M, Ilbawi AM, Anderson BO, Curigliano G: Global challenges and policy solutions in breast cancer control. Cancer Treat Rev 2022, 104:102339
2. Thu K, Soria-Bretones I, Mak T, Cescon D: Targeting the cell cycle in breast cancer: towards the next phase. Cell Cycle 2018, 17: 1871–1885
3. Maharjan CK, Mo J, Wang L, Kim M-C, Wang S, Borcherding N, Vikas P, Zhang W: Natural and synthetic estrogens in chronic inflammation and breast cancer. Cancers (Basel) 2021, 14:206
4. Schuler LA, Murdoch FE: Endogenous and therapeutic estrogens: maestro conductors of the microenvironment of ER+ breast cancers. Cancers (Basel) 2021, 13:3725

5. Walker RA, Martin CV: The aged breast. J Pathol 2007, 211: 232−240
6. Brown KA, Iyengar NM, Zhou XK, Gucalp A, Subbaramaiah K, Wang H, Giri DD, Morrow M, Falcone DJ, Wendel NK, Winston LA, Pollak M, Dierickx A, Hudis CA, Dannenberg AJ: Menopause is a determinant of breast aromatase expression and its associations with BMI, inflammation, and systemic markers. J Clin Endocrinol Metab 2017, 102:1692−1701
7. Rusidzé M, Adlanmérini M, Chantalat E, Raymond-Letron I, Cayre S, Arnal JF, Deugnier MA, Lenfant F: Estrogen receptor-[alpha] signaling in post-natal mammary development and breast cancers. Cell Mol Life Sci 2021, 78:5681−5705
8. Doisneau-Sixou SF, Sergio CM, Carroll JS, Hui R, Musgrove EA, Sutherland RL: Estrogen and antiestrogen regulation of cell cycle progression in breast cancer cells. Endocr Relat Cancer 2003, 10: 179−186
9. Zhou W, Slingerland JM: Links between oestrogen receptor activation and proteolysis: relevance to hormone-regulated cancer therapy. Nat Rev Cancer 2014, 14:26−38
10. Song RX, Zhang Z, Chen Y, Bao Y, Santen RJ: Estrogen signaling via a linear pathway involving insulin-like growth factor I receptor, matrix metalloproteinases, and epidermal growth factor receptor to activate mitogen-activated protein kinase in MCF-7 breast cancer cells. Endocrinology 2007, 148:4091−4101
11. Santen RJ, Stuenkel CA, Yue W: Mechanistic effects of estrogens on breast cancer. Cancer J 2022, 28:224−240
12. Zhao H, Zhou L, Shangguan AJ, Bulun SE: Aromatase expression and regulation in breast and endometrial cancer. J Mol Endocrinol 2016, 57:R19−R33
13. Cuzick J, Sestak I, Cawthorn S, Hamed H, Holli K, Howell A, Forbes JF; IBIS-I Investigators: Tamoxifen for prevention of breast cancer: extended long-term follow-up of the IBIS-I breast cancer prevention trial. Lancet Oncol 2015, 16:67−75
14. Cummings SR, Eckert S, Krueger KA, Grady D, Powles TJ, Cauley JA, Norton L, Nickelsen T, Bjarnason NH, Morrow M, Lippman ME, Black D, Glusman JE, Costa A, Jordan VC: The effect of raloxifene on risk of breast cancer in postmenopausal women: results from the MORE randomized trial. JAMA 1999, 281: 2189−2197
15. Goss PE, Ingle JN, Alés-Martínez JE, Cheung AM, Chlebowski RT, Wactawski-Wende J, McTiernan A, Robbins J, Johnson KC, Martin LW, Winquist E, Sarto GE, Garber JE, Fabian CJ, Pujol P, Maunsell E, Farmer P, Gelmon KA, Tu D, Richardson H; NCIC CTG MAP.3 Study Investigators: Exemestane for breast-cancer prevention in postmenopausal women. N Engl J Med 2011, 364:2381−2391
16. Olin JL, St Pierre M: Aromatase inhibitors in breast cancer prevention. Ann Pharmacother 2014, 48:1605−1610
17. Lazzeroni M, DeCensi A: Breast cancer prevention by antihormones and other drugs: where do we stand? Hematol Oncol Clin North Am 2013, 27:657−672
18. Fu X, De Angelis C, Schiff R: Interferon signaling in estrogen receptor−positive breast cancer: a revitalized topic. Endocrinology 2022, 163:bqab235
19. Dabydeen SA, Kang K, Díaz-Cruz ES, Alamri A, Axelrod ML, Bouker KB, Al-Kharboosh R, Clarke R, Hennighausen L, Furth PA: Comparison of tamoxifen and letrozole response in mammary preneoplasia of ER and aromatase overexpressing mice defines an immune-associated gene signature linked to tamoxifen resistance. Carcinogenesis 2015, 36:122−132
20. `Schwartz JL, Shajahan AN, Clarke R: The role of interferon regulatory factor-1 (IRF1) in overcoming antiestrogen resistance in the treatment of breast cancer. Int J Breast Cancer 2011, 2011: 912102
21. Choi HJ, Lui A, Ogony J, Jan R, Sims PJ, Lewis-Wambi J: Targeting interferon response genes sensitizes aromatase inhibitor resistant breast cancer cells to estrogen-induced cell death. Breast Cancer Res 2015, 17:6
22. Vieira AF, Schmitt F: An update on breast cancer multigene prognostic tests—emergent clinical biomarkers. Front Med (Lausanne) 2018, 5:248
23. Zeng C, Zhang J: A narrative review of five multigenetic assays in breast cancer. Transl Cancer Res 2022, 11:897−907
24. Ren X, Song Y, Zhang Y, Wu H, Chen L, Pang J, Zhou L, Shen S, Liang Z: Prognostic significance of different molecular typing methods and immune status based on RNA sequencing in HR-positive and HER2-negative early-stage breast cancer. BMC Cancer 2022, 22:548
25. Lænkholm A-V, Jensen M-B, Eriksen JO, Rasmussen BB, Knoop AS, Buckingham W, Ferree S, Schaper C, Nielsen TO, Haffner T, Kibøl T, Møller Talman M-L, Bak Jylling AM, Tabor TP, Ejlertsen B: PAM50 risk of recurrence score predicts 10-year distant recurrence in a comprehensive Danish cohort of postmenopausal women allocated to 5 years of endocrine therapy for hormone receptor−positive early breast cancer. J Clin Oncol 2018, 36: 735−740
26. Behravan H, Hartikainen JM, Tengström M, Kosma V-M, Mannermaa A: Predicting breast cancer risk using interacting genetic and demographic factors and machine learning. Sci Rep 2020, 10: 11044
27. Shrestha A, Cullinane C, Evoy D, Geraghty J, Rothwell J, Walshe J, McCartan D, McDermott E, Prichard R: Clinical treatment score post-5 years as a predictor of late distant recurrence in hormone receptor-positive breast cancer: systematic review and meta-analysis. Br J Surg 2022, 109:411−417
28. Alothman SJ, Kang K, Liu X, Krawczyk E, Azhar RI, Hu R, Goerlitz D, Kallakury BV, Furth PA: Characterization of transcriptome diversity and in vitro behavior of primary human high-risk breast cells. Sci Rep 2022, 12:6159
29. Herschkowitz JI, Simin K, Weigman VJ, Mikaelian I, Usary J, Hu Z, Rasmussen KE, Jones LP, Assefnia S, Chandrasekharan S, Backlund MG, Yin Y, Khramtsov AI, Bastein R, Quackenbush J, Glazer RI, Brown PH, Green JE, Kopelovich L, Furth PA, Palazzo JP, Olopade OI, Bernard PS, Churchill GA, Van Dyke T, Perou CM: Identification of conserved gene expression features between murine mammary carcinoma models and human breast tumors. Genome Biol 2007, 8:R76
30. Desai KV, Xiao N, Wang W, Gangi L, Greene J, Powell JI, Dickson R, Furth P, Hunter K, Kucherlapati R, Simon R, Liu ET, Green JE: Initiating oncogenic event determines gene-expression patterns of human breast cancer models. Proc Natl Acad Sci U S A 2002, 99:6967−6972
31. Furth PA, Cabrera MC, Díaz-Cruz ES, Millman S, Nakles RE: Assessing estrogen signaling aberrations in breast cancer risk using genetically engineered mouse models. Ann N Y Acad Sci 2011, 1229:147−155
32. Dabydeen SA, Furth PA: Genetically engineered ER[alpha]-positive breast cancer mouse models. Endocr Relat Cancer 2014, 21: R195−R208
33. Kirma NB, Tekmal RR: Transgenic mouse models of hormonal mammary carcinogenesis: advantages and limitations. Steroid Biochem Mol Biol 2012, 131:76−82
34. Díaz-Cruz ES, Sugimoto Y, Gallicano GI, Brueggemeier RW, Furth PA: Comparison of increased aromatase versus ER[alpha] in the generation of mammary hyperplasia and cancer. Cancer Res 2011, 71:5477−5487
35. Miermont AM, Cabrera MC, Frech SM, Nakles RE, Diaz-Cruz ES, Shiffert MT, Furth PA: Association of over-expressed estrogen receptor alpha with development of tamoxifen resistant hyperplasia and adenocarcinomas in genetically engineered mice. Anat Physiol 2012, (Suppl 12):001
36. Miermont AM, Parrish AR, Furth PA: Role of ER[alpha] in the differential response of Stat5a loss in susceptibility to mammary preneoplasia and DMBA-induced carcinogenesis. Carcinogenesis 2010, 31:1124−1131

37. Karantza V: Keratins in health and cancer: more than mere epithelial cell markers. Oncogene 2011, 30:127−138
38. Shao MM, Chan SK, Yu AM, Lam CC, Tsang JY, Lui PC, Law BK, Tan PH, Tse GM: Keratin expression in breast cancers. Virchows Arch 2012, 461:313−322
39. Mikaelian I, Hovick M, Silva KA, Burzenski LM, Shultz LD, Ackert-Bicknell CL, Cox GA, Sundberg JP: Expression of terminal differentiation proteins defines stages of mouse mammary gland development. Vet Pathol 2006, 43:36−49
40. Alam H, Sehgal L, Kundu ST, Dalal SN, Vaidya MM: Novel function of keratins 5 and 14 in proliferation and differentiation of stratified epithelial cells. Mol Biol Cell 2011, 22:4068−4078
41. Payne AH, Hales DB: Overview of steroidogenic enzymes in the pathway from cholesterol to active steroid hormones. Endocr Rev 2004, 25:947−970
42. Gonsioroski A, Meling DD, Gao L, Plewa MJ, Flaws JA: Iodoacetic acid affects estrous cyclicity, ovarian gene expression, and hormone levels in mice. Biol Reprod 2021, 105:1030−1042
43. Rattan S, Brehm E, Gao L, Niermann S, Flaws JA: Prenatal exposure to di(2-ethylhexyl) phthalate disrupts ovarian function in a transgenerational manner in female mice. Biol Reprod 2018, 98: 130−145
44. Tu X, Kuang Z, Gong X, Shi Y, Yu L, Shi H, Wang J, Sun Z: The influence of LepR tyrosine site mutations on mouse ovary development and related gene expression changes. PLoS One 2015, 10: e0141800
45. Anderson WF, Rosenberg PS, Prat A, Perou CM, Sherman ME: How many etiological subtypes of breast cancer: two, three, four, or more? J Natl Cancer Inst 2014, 106:dju165
46. Witherby SM, Muss HB: Managing early-stage breast cancer in your older patients. Oncology (Williston Park) 2006, 20:1003−1012
47. Kamińska M, Ciszewski T, Łopacka-Szatan K, Miotła P, Starosławska E: Breast cancer risk factors. Prz Menopauzalny 2015, 14:196−202
48. Aapro M, Wildiers H: Triple-negative breast cancer in the older population. Ann Oncol 2012, 23(Suppl 6):vi52−vi55
49. Barginear MF, Muss H, Kimmick G, Owusu C, Mrozek E, Shahrokni A, Ballman K, Hurria A: Breast cancer and aging: results of the U13 conference breast cancer panel. Breast Cancer Res Treat 2014, 146:1−6
50. Cappellani A, Vita MD, Zanghì A, Cavallaro A, Piccolo G, Majorana M, Barbera G, Berretta M: Prognostic factors in elderly patients with breast cancer. BMC Surg 2013, 13:S2
51. LaBarge MA, Mora-Blanco EL, Samson S, Miyano M: Breast cancer beyond the age of mutation. Gerontology 2016, 62:434−442
52. Diaz-Cruz ES, Cabrera MC, Nakles R, Rutstein BH, Furth PA: BRCA1 deficient mouse models to study pathogenesis and therapy of triple negative breast cancer. Breast Dis 2010, 32:85−97
53. Gu Y, Bui T, Muller WJ: Exploiting mouse models to recapitulate clinical tumor dormancy and recurrence in breast cancer. Endocrinology 2022, 163:bqac055
54. Sflomos G, Schipper K, Koorman T, Fitzpatrick A, Oesterreich S, Lee AV, Jonkers J, Brunton VG, Christgen M, Isacke C, Derksen PWB, Brisken C: Atlas of lobular breast cancer models: challenges and strategic directions. Cancers (Basel) 2021, 13:5396
55. Lin DI, Lessie MD, Gladden AB, Bassing CH, Wagner K-U, Diehl JA: Disruption of cyclin D1 nuclear export and proteolysis accelerates mammary carcinogenesis. Oncogene 2008, 27: 1231−1242
56. Nakles RE, Shiffert MT, Díaz-Cruz ES, Cabrera MC, Alotaiby M, Miermont AM, Riegel AT, Furth PA: Altered AIB1 or AIB1Δ3 expression impacts ER[alpha] effects on mammary gland stromal and epithelial content. Mol Endocrinol 2011, 25:549−563
57. Rose-Hellekant TA, Arendt LM, Schroeder MD, Gilchrist K, Sandgren EP, Schuler LA: Prolactin induces ER[alpha]-positive and ER[alpha]-negative mammary cancer in transgenic mice. Oncogene 2003, 22:4664−4674
58. Chan SR, Vermi W, Luo J, Lucini L, Rickert C, Fowler AM, Lonardi S, Arthur C, Young LJ, Levy DE, Welch MJ, Cardiff RD, Schreiber RD: STAT1-deficient mice spontaneously develop estrogen receptor [alpha]-positive luminal mammary carcinomas. Breast Cancer Res 2012, 14:R16
59. Hruska KS, Tilli MT, Ren S, Cotarla I, Kwong T, Li M, Fondell JD, Hewitt JA, Koos RD, Furth PA, Flaws JA: Conditional overexpression of estrogen receptor alpha in a transgenic mouse model. Transgenic Res 2002, 11:361−372
60. Li M, Hu J, Heermeier K, Hennighausen L, Furth PA: Apoptosis and remodeling of mammary gland tissue during involution proceeds through p53-independent pathways. Cell Growth Differ 1996, 7:13−20
61. Alothman SJ, Wang W, Goerlitz DS, Islam M, Zhong X, Kishore A, Azhar RI, Kallakury BV, Furth PA: Responsiveness of Brca1 and Trp53 deficiency induced mammary preneoplasia to selective estrogen modulators versus an aromatase inhibitor in Mus musculus. Cancer Prev Res (Phila) 2017, 10:244−254
62. Nakles RE, Kallakury BVS, Furth PA: The PPAR[gamma] agonist efatutazone increases the spectrum of well-differentiated mammary cancer subtypes initiated by loss of full-length BRCA1 in association with TP53 haploinsufficiency. Am J Pathol 2013, 182:1976−1985
63. Medina D: Premalignant and malignant mammary lesions induced by MMTV and chemical carcinogens. J Mammary Gland Biol Neoplasia 2008, 13:271−277
64. Rooney BL, Rooney BP, Muralidaran V, Wang W, Furth PA: Mouse mammary gland whole mount density assessment across different morphologies using a bifurcated program for image processing. Am J Pathol 2022, 192:1407−1417
65. Dobin A, Davis CA, Schlesinger F, Drenkow J, Zaleski C, Jha S, Batut P, Chaisson M, Gingeras TR: STAR: ultrafast universal RNA-seq aligner. Bioinformatics 2013, 29:15−21
66. Risso D, Ngai J, Speed TP, Dudoit S: Normalization of RNA-seq data using factor analysis of control genes or samples. Nat Biotechnol 2014, 32:896−902
67. Li B, Dewey CN: RSEM: accurate transcript quantification from RNA-Seq data with or without a reference genome. BMC Bioinformatics 2011, 12:323
68. Love MI, Huber W, Anders S: Moderated estimation of fold change and dispersion for RNA-seq data with DESeq2. Genome Biol 2014, 15:550
69. Subramanian A, Tamayo P, Mootha VK, Mukherjee S, Ebert BL, Gillette MA, Paulovich A, Pomeroy SL, Golub TR, Lander ES, Mesirov JP: Gene set enrichment analysis: a knowledge-based approach for interpreting genome-wide expression profiles. Proc Natl Acad Sci U S A 2005, 102:15545−15550
70. Liberzon A, Birger C, Thorvaldsdóttir H, Ghandi M, Mesirov JP, Tamayo P: The Molecular Signatures Database (MSigDB) hallmark gene set collection. Cell Syst 2015, 1:417−425
71. Yoo KH, Oh S, Kang K, Hensel T, Robinson GW, Hennighausen L: Loss of EZH2 results in precocious mammary gland development and activation of STAT5-dependent genes. Nucleic Acids Res 2015, 43: 8774−8789
72. Edgar R, Domrachev M, Lash AE: Gene Expression Omnibus: NCBI gene expression and hybridization array data repository. Nucleic Acids Res 2002, 30:207−210
73. Flurkey K, Currer JM, Harrison DE: Mouse models in aging research. Edited by Fox JG, Davisson MT, Quimby FW, Barthold SW, Newcomer CE, Smith AL. In The Mouse in Biomedical Research (Second Edition) History, Wild Mice, and Genetics. ed 2. Burlington, MA: American College of Laboratory Animal Medicine (Elsevier), 2007. pp. 637−672
74. Parks RM, Alfarsi LH, Green AR, Cheung KL: Biology of primary breast cancer in older women beyond routine biomarkers. Breast Cancer 2021, 28:991−1001
75. Tarone RE, Chu KC: The greater impact of menopause on ER- than ER+ breast cancer incidence: a possible explanation (United States). Cancer Causes Control 2002, 13:7−14

76. Porras L, Ismail H, Mader S: Positive regulation of estrogen receptor alpha in breast tumorigenesis. Cells 2021, 10:2966
77. Ali S, Coombes RC: Estrogen receptor alpha in human breast cancer: occurrence and significance. J Mammary Gland Biol Neoplasia 2000, 5:271−281
78. Gérard C, Brown KA: Obesity and breast cancer − role of estrogens and the molecular underpinnings of aromatase regulation in breast adipose tissue. Mol Cell Endocrinol 2018, 466:15−30
79. Kulendran M, Salhab M, Mokbel K: Oestrogen-synthesising enzymes and breast cancer. Anticancer Res 2009, 29:1095−1109
80. Frech MS, Halama ED, Tilli MT, Singh B, Gunther EJ, Chodosh LA, Flaws JA, Furth PA: Deregulated estrogen receptor alpha expression in mammary epithelial cells of transgenic mice results in the development of ductal carcinoma in situ. Cancer Res 2005, 65:681−685
81. Walters KA, Rodriguez Paris V, Aflatounian A, Handelsman DJ: Androgens and ovarian function: translation from basic discovery research to clinical impact. J Endocrinol 2019, 242:R23−R50
82. Oakes SR, Hilton HN, Ormandy CJ: Key stages in mammary gland development - the alveolar switch: coordinating the proliferative cues and cell fate decisions that drive the formation of lobuloalveoli from ductal epithelium. Breast Cancer Res 2006, 8:207
83. Bhat D: The "why and how" of cervical cancers and genital HPV infection. Cytojournal 2022, 19:22
84. Ruiz R, Herrero C, Strasser-Weippl K, Touya D, Louis JS, Bukowski A, Goss PE: Epidemiology and pathophysiology of pregnancy-associated breast cancer: a review. Breast 2017, 35:136−141
85. Lefrère H, Lenaerts L, Borges VF, Schedin P, Neven P, Amant F: Postpartum breast cancer: mechanisms underlying its worse prognosis, treatment implications, and fertility preservation. Int J Gynecol Cancer 2021, 31:412−422
86. Haricharan S, Dong J, Hein S, Reddy JP, Du Z, Toneff M, Holloway K, Hilsenbeck SG, Huang S, Atkinson R, Woodward W, Jindal S, Borges VF, Gutierrez C, Zhang H, Schedin PJ, Osborne CK, Tweardy DJ, Li Y: Mechanism and preclinical prevention of increased breast cancer risk caused by pregnancy. Elife 2013, 2:e00996
87. Zhou Y, Eppenberger-Castori S, Eppenberger U, Benz CC: The NFkappaB pathway and endocrine-resistant breast cancer. Endocr Relat Cancer 2005, 12(Suppl 1):S37−S46